U. of Iowa 71:4

Double Probe Measurements of DC Electric Fields with the Injun 5 Satellite

by

David P. Cauffman
and
Donald A. Gurnett

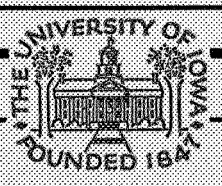

This work was supported in part by the Office of Naval Research under Contract No. N00014-68-A-0196-0003

Department of Physics and Astronomy
THE UNIVERSITY OF IOWA
Iowa City, Iowa

Double Probe Measurements of DC Electric Fields with the Injun 5 Satellite

by

David P. Cauffman
and
Donald A. Gurnett

Department of Physics and Astronomy
The University of Iowa
Iowa City, Iowa 52240

January 1971

Research supported in part by the National Aeronautics and Space Administration under contracts NAS5-10625, NAS1-8141, NAS1-8144(f), NAS1-8150(f), and NGL-16-001-043(97); and by the Office of Naval Research under contract N00014-68-A-0196-0003.

UNCLASSIFIED

Security Classification

DOCUMENT CONTROL DATA - R&D

(Security classification of title, body of abstract and indexing annotation must be entered when the overall report is classified)

1. ORIGINATING ACTIVITY *(Corporate author)*

Department of Physics and Astronomy
University of Iowa

2a. REPORT SECURITY CLASSIFICATION

UNCLASSIFIED

2b. GROUP

3. REPORT TITLE

"Double Probe Measurements of DC Electric Fields with the Injun 5 Satellite"

4. DESCRIPTIVE NOTES *(Type of report and inclusive dates)*

Progress, January 1971

5. AUTHOR(S) *(Last name, first name, initial)*

Cauffman, David P., and Donald A. Gurnett

6. REPORT DATE	7a. TOTAL NO. OF PAGES	7b. NO. OF REFS
January 1971	73	34

8a. CONTRACT OR GRANT NO.	9a. ORIGINATOR'S REPORT NUMBER(S)
N00014-68-A-0196-0003	U of Iowa 71-4
b. PROJECT NO.	
c.	9b. OTHER REPORT NO(S) *(Any other numbers that may be assigned this report)*
d.	

10. AVAILABILITY/LIMITATION NOTICES

Distribution of this document is unlimited.

11. SUPPLEMENTARY NOTES	12. SPONSORING MILITARY ACTIVITY
	Office of Naval Research

13. ABSTRACT

[see following page]

DD FORM 1 JAN 64 1473

UNCLASSIFIED

Security Classification

14. KEY WORDS	LINK A		LINK B		LINK C	
	ROLE	WT	ROLE	WT	ROLE	WT
Magnetospheric Electric Fields						
Double Probe Electric Field Measurements						
DC Electric Fields						

INSTRUCTIONS

1. ORIGINATING ACTIVITY: Enter the name and address of the contractor, subcontractor, grantee, Department of Defense activity or other organization *(corporate author)* issuing the report.

2a. REPORT SECURITY CLASSIFICATION: Enter the overall security classification of the report. Indicate whether "Restricted Data" is included. Marking is to be in accordance with appropriate security regulations.

2b. GROUP: Automatic downgrading is specified in DoD Directive 5200.10 and Armed Forces Industrial Manual. Enter the group number. Also, when applicable, show that optional markings have been used for Group 3 and Group 4 as authorized.

3. REPORT TITLE: Enter the complete report title in all capital letters. Titles in all cases should be unclassified. If a meaningful title cannot be selected without classification, show title classification in all capitals in parenthesis immediately following the title.

4. DESCRIPTIVE NOTES: If appropriate, enter the type of report, e.g., interim, progress, summary, annual, or final. Give the inclusive dates when a specific reporting period is covered.

5. AUTHOR(S): Enter the name(s) of author(s) as shown on or in the report. Enter last name, first name, middle initial. If military, show rank and branch of service. The name of the principal author is an absolute minimum requirement.

6. REPORT DATE: Enter the date of the report as day, month, year; or month, year. If more than one date appears on the report, use date of publication.

7a. TOTAL NUMBER OF PAGES: The total page count should follow normal pagination procedures, i.e., enter the number of pages containing information.

7b. NUMBER OF REFERENCES: Enter the total number of references cited in the report.

8a. CONTRACT OR GRANT NUMBER: If appropriate, enter the applicable number of the contract or grant under which the report was written.

8b, 8c, & 8d. PROJECT NUMBER: Enter the appropriate military department identification, such as project number, subproject number, system numbers, task number, etc.

9a. ORIGINATOR'S REPORT NUMBER(S): Enter the official report number by which the document will be identified and controlled by the originating activity. This number must be unique to this report.

9b. OTHER REPORT NUMBER(S): If the report has been assigned any other report numbers *(either by the originator or by the sponsor)*, also enter this number(s).

10. AVAILABILITY/LIMITATION NOTICES: Enter any limitations on further dissemination of the report, other than those imposed by security classification, using standard statements such as:

(1) "Qualified requesters may obtain copies of this report from DDC."

(2) "Foreign announcement and dissemination of this report by DDC is not authorized."

(3) "U. S. Government agencies may obtain copies of this report directly from DDC. Other qualified DDC users shall request through _____."

(4) "U. S. military agencies may obtain copies of this report directly from DDC. Other qualified users shall request through _____."

(5) "All distribution of this report is controlled. Qualified DDC users shall request through _____."

If the report has been furnished to the Office of Technical Services, Department of Commerce, for sale to the public, indicate this fact and enter the price, if known.

11. SUPPLEMENTARY NOTES: Use for additional explanatory notes.

12. SPONSORING MILITARY ACTIVITY: Enter the name of the departmental project office or laboratory sponsoring *(paying for)* the research and development. Include address.

13. ABSTRACT: Enter an abstract giving a brief and factual summary of the document indicative of the report, even though it may also appear elsewhere in the body of the technical report. If additional space is required, a continuation sheet shall be attached.

It is highly desirable that the abstract of classified reports be unclassified. Each paragraph of the abstract shall end with an indication of the military security classification of the information in the paragraph, represented as *(TS)*, *(S)*, *(C)*, *or (U)*.

There is no limitation on the length of the abstract. However, the suggested length is from 150 to 225 words.

14. KEY WORDS: Key words are technically meaningful terms or short phrases that characterize a report and may be used as index entries for cataloging the report. Key words must be selected so that no security classification is required. Identifiers, such as equipment model designation, trade name, military project code name, geographic location, may be used as key words but will be followed by an indication of technical context. The assignment of links, roles, and weights is optional.

ABSTRACT

This paper reports on the operation and results of the double-probe DC electric field experiment on the low altitude polar orbiting Injun 5 satellite. At middle and low latitudes, where the convection electric field is generally very small, the operation of the double-probe electric field antenna is investigated by comparing measured electric fields with the $\vec{V}_s x \vec{B}$ electric field generated by the satellite motion through the ionosphere. Errors caused by sunlight shadows on the probes, wake effects, and antenna impedance variations are discussed.

At high latitudes convection electric fields greater than 30 mV/meter, and sometimes greater than 100 mV/meter, are frequently observed in the auroral zone. A common feature of these high latitude convection fields is the occurrence of abrupt reversals in the east-west convection velocity at auroral zone latitudes. For dusk-dawn local times, these reversals generally correspond to an east-west flow away from the sun on the high latitude side of the reversal and toward the sun on the low latitude side. Over the polar region above the auroral zone the convection velocity is usually

small. At the plasmapause/light ion trough boundary small, 10 to 20 mV/meter, electric field perturbations are sometimes observed, corresponding to generally westward convection outside the plasmasphere.

At high altitudes, above about 1500 km, over the auroral zone/polar cap regions irregular electric field "noise" with amplitudes from 10 to 30 mV/meter is consistently observed. Possible explanations of the high altitude electric field noise are discussed.

Results are consistent with measurements using the barium cloud drift technique. Convection observed is also compared with models of magnetospheric structure and with models of substorms and aurorae.

I. INTRODUCTION

The importance of electric field measurements for studying the convection of plasma in the magnetosphere has been recognized for a number of years [Dungey, 1961; Axford and Hines, 1961; Piddington, 1962; Boström, 1967; and Axford, 1969]; however, only recently have techniques been developed for the measurement of magnetospheric electric fields. These techniques include (1) observations of the drift of artificial barium cloud releases [Haerendel et al., 1967; Föppl et al., 1968; and Wescott et al., 1969], (2) direct probe measurements using rockets and satellites [Mozer and Bruston, 1967; Fahleson et al., 1968; Heppner et al., 1968; Gurnett, 1970; Maynard and Heppner, 1970; and Potter, 1970], (3) subionospheric electric field measurements with high altitude balloons [Mozer and Serlin, 1969], and (4) various other more indirect methods such as observations of whistler duct motions [Carpenter, 1970], and charged particle energy spectrum observations [Van Allen, 1970]. Of these techniques, probably the most extensive and sensitive measurements have been obtained from artificial barium cloud releases. Satellite measurements can, of course, provide much more extensive spatial coverage and quantities of data than is possible with

either sounding rockets or barium cloud releases. This paper reports on initial results from the DC electric field experiment on the low altitude (677 to 2528 km) polar orbiting Injun 5 satellite.

II. DESCRIPTION OF THE EXPERIMENT

A. Instrumentation

The electric field sensors on Injun 5 consist of two conducting spheres 20.3 cm in diameter mounted on booms as shown in Figure 1. The spheres, which are made of aluminum, are coated with a conducting silver paint to provide a uniform conducting surface. The aluminum booms supporting the spheres are insulated from the spheres and coated with a non-conducting paint to insulate the booms from the surrounding plasma. The center to center distance between the spheres is 2.85 meters. The spacecraft is magnetically oriented by a bar magnet within the spacecraft such that when properly aligned the x-axis of the spacecraft is parallel to the geomagnetic field with the positive x-axis pointing downward in the northern hemisphere. Typical maximum alignment errors between the x-axis and the geomagnetic field are about 10 to 15 degrees. As shown in Figure 1, when the spacecraft is magnetically oriented, the DC electric field experiment is sensitive to the electric field, $E_{\perp}$, perpendicular to the geomagnetic field.

Ideally, the two spheres and supporting booms should have exactly the same (translational) geometry so that

sunlight and ram ion shadowing of the spheres by the booms is the same for both spheres, thereby eliminating errors due to dissimilar sheath characteristics for the two spheres. Unfortunately, structural limitations did not permit adding stub booms, as suggested by Fahleson [1967], to maintain identical particle and sunlight shadowing for all orientations. Errors in the measurement due to asymmetrical shadowing of the two spheres are discussed in section III.

The potential difference between the two spheres is determined using a high input impedance differential amplifier located in the main spacecraft electronics. The differential amplifier has a dynamic range of ±1.0 volts and an RC time constant of 0.4 seconds. The output from the differential amplifier is sampled by the digital data system once every 4 seconds. The minimum resolvable electric field strength increment is approximately 2.75 mV/meter.

In order to minimize errors due to voltage drops through the plasma sheath surrounding each sphere, the differential amplifier input impedance must be much larger than the sheath impedance. The input impedance of the differential amplifier is 20 megohms from each sphere to the spacecraft body. This input impedance is much larger than the sheath resistances generally encountered in the Injun 5 orbit. In order to verify that the sheath resistance is small compared to the input impedance of the differential amplifier, the average AC impedance

of the two spheres is measured every 30 seconds by differentially driving the spheres with a constant amplitude AC current source (I=0.1 μamp RMS) and measuring the resulting AC potential difference between the spheres. Further details of the Injun 5 DC electric field experiment are given by Gurnett et al. [1969].

B. Theory of Operation

The theory of operation for the double probe type of electric field antenna used on Injun 5 has been discussed by Fahleson [1967] and Aggson [1966] and is summarized here to provide a basis for discussing the observed operation in orbit. The double probe antenna can be thought of as two high-impedance potential probes immersed in the highly conducting plasma surrounding the spacecraft. As is well known, an inhomogeneous plasma sheath forms around the entire spacecraft-probe system as illustrated in the top diagram of Figure 2. For the plasma densities found in the Injun 5 orbit, the sheath is normally a positive ion sheath with a characteristic thickness given by the Debye length [Fahleson, 1967]. In regions of very low plasma density the photo-electron current can, however, exceed the current collected from the plasma in which case a photo-electron sheath is formed with a characteristic thickness of about 20 cm [Aggson, 1966].

An equivalent circuit model of the coupling of the probe system to the plasma is shown in the bottom diagram of Figure 2. In this model the voltage sources $E(\ell/2)$ and $E(-\ell/2)$

represent the plasma potential at the center of the two spheres. For the Injun 5 orbit the sheath thickness is normally small compared to the antenna length. It is, therefore, expected that the effective length, ℓ, of the antenna will be equal to the center to center distance between the spheres. For a positive ion sheath the sheath resistance R_s and sheath potential V_s can be computed from Langmuir probe theory and are given by [Fahleson, 1967]

$$R_s = \frac{U_e}{I_i + I_p} \text{ , and} \tag{1}$$

$$V_s = -U_e \, \ell n\left(\frac{I_e}{I_i + I_p}\right) , \tag{2}$$

where U_e is the electron thermal potential ($U_e = kT_e/e$), I_e is the random electron current which would be collected by the sphere in the absence of sheath effects, I_i is the ion ram current incident on the spheres, and I_p is the photo-electron current emitted by the sphere.

If the electron density becomes so low that the electron current plus the bias current to the differential amplifier, I_B, is less than the photo-electron current plus the ion ram current ($I_e + I_B < I_p + I_i$) then the plasma sheath becomes a photo-electron sheath [Aggson, 1966].

For a photo-sheath the sheath potential, V_s, of the spheres is positive and the Langmuir probe relations given by

Equations (1) and (2) are no longer valid. If an exponential photo-electron energy spectrum is assumed, with an e-folding energy $U_p \simeq 3.0$ volts, then the sheath resistance, R_s, and sheath potential, V_s, for the photo-electron sheath are given by

$$R_s = \frac{U_p}{I_e - I_i} \text{ , and} \tag{3}$$

$$V_s = U_p \ell n \left(\frac{I_p}{I_e - I_i} \right). \tag{4}$$

These equations are valid whenever $I_e + I_B < I_p + I_i$.

The resistanee R_B im the equivalent circuit of Figure 2 represents the input resistance of the differential amplifier. From the circuit diagram it can be readily shown that the observed potential difference between the spheres is given by

$$V_+ - V_- = - \frac{E_y \ell}{2} \left[\frac{1}{1 + \frac{R_{s+}}{R_B}} + \frac{1}{1 + \frac{R_{s-}}{R_B}} \right] + \frac{V_{s+}}{1 + \frac{R_{s+}}{R_B}} - \frac{V_{s-}}{1 + \frac{R_{s-}}{R_B}} \text{ ,} \tag{5}$$

where the plus (+) and minus (-) subscripts refer to the +y and -y spheres, respectively. If the sheath voltages are the same for both spheres, $V_{s+} = V_{s-}$, and the sheath resistances are small compared to the differential amplifier input impedance (R_{s+}, $R_{s-} \ll R_B$) then the y component of the electric

field is directly proportional to the potential difference between the spheres,

$$E_y = - \frac{V_+ - V_-}{\ell} . \qquad (6)$$

In the following section the validity of the above equations, and the assumptions used in their derivations, are investigated using inflight observations of the electric antenna operation.

III. OPERATION OF THE ELECTRIC ANTENNA SYSTEM IN ORBIT

A. Comparison with $\vec{V}_s x \vec{B}$

At middle and low latitudes, where the ionospheric plasma is expected to co-rotate with the earth [Axford, 1969], only the $\vec{V}_s x \vec{B}$ electric field arising from the satellite velocity $\vec{V}_s$ through the ionosphere should be observed. Thus, at middle and low latitudes it is possible to "calibrate" the electric field measurement by comparing the observed electric field with the computed $\vec{V}_s x \vec{B}$ electric field.

The E_y electric field observed for a typical Injun 5 orbit is shown in Figure 3, as determined from the sphere potential difference using Equation (6). The systematic sinusoidal variation evident in the measured electric field, with a period of about 20 minutes, is caused by the $\vec{V}_s x \vec{B}$ electric field. The sinusoidal modulation of the observed $\vec{V}_s x \vec{B}$ electric field is due to the slow rotation of the satellite around the geomagnetic field with a period of about 20 minutes. Because the magnetic orientation always maintains the electric antenna axis perpendicular to the geomagnetic field, the maxima and minima in the measured $\vec{V}_s x \vec{B}$ electric field occur when the antenna axis is parallel with the $\vec{V}_s x \vec{B}$ electric field. At these points the measured $\vec{V}_s x \vec{B}$ electric field can be

compared directly with the magnitude of the computed $\vec{V}_s x \vec{B}$ field. The dashed lines in Figure 3 are the positive and negative limits of the $\vec{V}_s x \vec{B}$ field as computed from the satellite orbit. The satellite velocity $\vec{V}_s$ was computed relative to a coordinate system co-rotating with the earth and the geomagnetic field was computed using the 1965 Cain et al. [1967] expansion for the geomagnetic field. Near the magnetic equator the $\vec{V}_s x \vec{B}$ field becomes very small as the angle between the satellite velocity vector and the geomagnetic field becomes small.

Discounting the spacecraft wake and shadow effects indicated in Figure 3, the maxima and minima in the observed $\vec{V}_s x \vec{B}$ electric field at middle and low latitudes are observed to fit the dotted $|\vec{V}_s x \vec{B}|$ envelope to within about 50 mV/meter. Similar comparisons on other orbits indicate that the maximum error between the computed and measured $\vec{V}_s x \vec{B}$ field, when spacecraft wake and shadow effects are eliminated, is typically about 50 mV/meter. As discussed in the following sections, this error is believed to be primarily due to asymmetrical sunlight shadowing of the spheres by the supporting booms.

B. Sheath Resistance

The bottom plot of Figure 3 shows the electric antenna impedance for an entire orbit at a frequency of 30 Hz. At this low frequency the antenna impedance is observed to be almost purely resistive [Gurnett, et al., 1969]. This

resistive impedance is believed to be almost entirely due to the plasma sheath surrounding the spheres.

The sheath resistance is observed to vary widely during an orbit, from less than 10^4 ohms at low altitudes near the magnetic equator, to greater than 10^6 ohms at high altitudes over the polar regions. These variations can be generally understood from Equation (1) for the resistance of the plasma sheath surrounding the spheres.

At low altitudes, where the electron number density, N_e, exceeds about 7×10^4 electrons/cm^3, the ram ion current exceeds the photo-electron current ($I_i > I_p$), and the sheath resistance given by Equation (1) becomes inversely proportional to the electron number density ($I_i \propto N_e$). The sheath resistances less than 10^5 ohms, evident at low altitudes near the magnetic equator in Figure 3, are due to the increased electron density in this region. The sheath resistance decrease at low altitudes is particularly pronounced when the perigee is near the magnetic equator where the latitudinal maximum in the electron density occurs [Brace *et al.*, 1967]. The sheath resistance is often less than 10^4 ohms in this region [see Figure 6 of Gurnett *et al.*, 1969].

At higher altitudes, where the electron density is less than about 7×10^4 electrons/cm^3, the ram ion current is less than the photo-electron current ($I_i < I_p$). Under these conditions the sheath resistance as given by Equation (1)

is determined primarily by the electron temperature. An electron temperature of 2500°K, which is typical for the Injun 5 orbit at mid and low latitudes and a photo-electron current estimated to be about 2.5 μamps, gives a sheath resistance of $\sim 10^5$ ohms. This value is typical of the sheath resistances actually observed at mid and low latitudes above about 1000 km altitude and accounts for the general magnitude of the sheath resistances most commonly observed with Injun 5.

The increased sheath resistance evident in Figure 3 at high altitudes over the northern polar region is believed to be due to the increased electron temperature in this region ($R_s \approx kT_e/eI_p$) or due to the formation of a photo-sheath in regions of unusually low electron density (see discussions of wake effects in section D).

An abrupt change in the sheath resistance is commonly observed as the spacecraft crosses the plasmapause/light ion trough boundary, with larger sheath resistances being observed outside the plasmasphere [see Figure 5 of Gurnett et al., 1969]. This increased sheath resistance is believed to be due to the increase in the electron temperature and the decrease in the ion ram current on the high latitude side of the plasmapause boundary.

When the spacecraft is in darkness at high altitudes (above 2000 km) the sheath resistance often exceeds 10^6 ohms. This large sheath resistance occurs because both the photo-

electron current, I_p, and the ion ram current, I_i, in the denominator of Equation (1) are small when the spacecraft is in darkness at high altitudes.

Typically the sheath resistances observed in flight are less than 10^6 ohms so that corrections to the electric field determinations due to the finite differential amplifier input impedance (R_B=2×10^7 ohms) are usually negligible. However, at high altitudes when the spacecraft is in darkness or is over the polar regions, the sheath resistance sometimes exceeds 10^6 ohms. In these cases, which are readily identified from the impedance measurement data, significant errors due to the finite differential amplifier input impedance can occur.

C. Sunlight Shadowing Effects

The abrupt jumps in the sphere potential difference labeled "spacecraft shadow" in Figure 3 are due to the change in the photo-electron emission of one of the spheres as the sphere passes through the sunlight shadow of the spacecraft body. The potential of the shadowed sphere typically decreases by about 0.3 to 0.5 volts as the sphere passes through the shadowed region. The origin of this shadowing effect can be seen from Equation (2) for the sheath potential. If the photo-electron currents are identical for both spheres, then the sheath potentials V_{s+} and V_{s-} are equal and cancel out of Equation (5) for the sphere potential difference (assuming

that R_{s+}, $R_{s-} << R_B$). However, any difference in the photo-electron current emitted by the two spheres, such as is caused by sunlight shadowing of one of the spheres, will cause an imbalance of the two sheath potentials and a corresponding shift in the sphere potential difference. The polarities are such that when the +y sphere is shadowed, the E_y component of the electric field increases. The range of sun directions ($\vec{S}$) for which shadowing can occur for each sphere is indicated in Figure 1. Sunlight shadowing effects caused by the spacecraft body are usually easy to identify because of their distinctive characteristics and predictable occurrence.

The photo-electron current emitted by the sphere can be determined from the jump, ΔV_s, in the sphere potential difference as the sphere is shadowed. A rough estimate of the photo-electron current can be made from the "Ohms law" relation $I_p = \Delta V_s / R_s$, which for a typical case of $\Delta V_s = 0.3$ volts and $R_s = 10^5$ ohms, gives $I_p \simeq 3$ μamp. A more complete analysis, which takes into account the nonlinear sheath characteristics has been performed using the Langmuir probe equations given by Fahleson [1967] and gives a value for the photo-electron current of $I_p = 2.5 \pm 1.0$ μamp.

Asymmetrical sunlight shadowing effects by the booms supporting the spheres are believed to be primarily responsible for the errors in the $\vec{V}_s \times \vec{B}$ "calibration" comparisons discussed earlier. Since the boom can at most shadow only about 12%

of the projected area of a sphere, the magnitude of the boom shadowing effects are proportionately smaller than the spacecraft body shadowing effects. The maximum error due to boom shadowing is estimated to be about 50 mV/meter. Since boom shadowing can occur to varying degrees over a large range of spacecraft orientations (see Figure 1), this type of error is present in a large fraction of the Injun 5 data. In contrast to the spacecraft body shadows which produce abrupt jumps in the sphere potential difference the boom shadow error is a smoothly varying function of the spacecraft orientation with a time scale comparable to the rotation period of the spacecraft. The tendency for the measured $\vec{V}_s x \vec{B}$ electric field in Figure 3 to undershoot the $|\vec{V}_s x \vec{B}|$ envelope in the southern hemisphere and overshoot in the northern hemisphere can be accounted for by a detailed consideration of the polarity of the boom shadowing errors in the northern and southern hemisphere. (In this case the boom shadowing error for a given orientation has the same sign in either hemisphere, but the vector direction of $\vec{V}_s x \vec{B}$ is reversed. The boom shadowing error therefore adds to $\vec{V}_s x \vec{B}$ in one hemisphere and subtracts in the opposite hemisphere.) Although it has not been considered practical to quantitatively correct for boom shadowing errors as part of the routine data processing, it is usually easy to distinguish boom shadowing errors from magnetospheric electric fields on

the basis of the time scales involved. Also, there is a fairly large range of orientations for which no boom shadowing can occur for either sphere (see Figure 1).

D. Wake Effects

Perturbations due to a wake from the spacecraft body have been observed in the Injun 5 DC electric field data. Because of the magnetic orientation and geometry of the electric antenna, wake effects are expected for Injun 5 only at high latitudes. Three exceptionally clear examples of wakes observed on successive passes over the northern polar region are shown in Figure 4. The electric field plotted in Figure 4 is the difference between the observed electric field and the best estimate of the $\vec{V}_s x \vec{B}$ electric field. The angle between the anti-velocity vector ($-\vec{V}_s$) and the position vector of the +y sphere relative to the center of the spacecraft body is also shown in Figure 4. The electric field perturbation observed for these three cases is seen to correlate well with the position of the sphere with respect to the anti-velocity vector direction. The angular width of the wake region is very large, from $\pm 60°$ to $\pm 90°$ in these cases. Since the E_y electric field perturbation is negative when the +y sphere is in the wake, it follows from Equation (6) that the potential of the +y sphere must <u>increase</u> in the wake region.

Wake effects are observed with Injun 5 only at high latitudes, above 60° invariant latitude. In order to provide further information on the origin of the wake effects observed, a study was performed on the occurrence of wakes as a function of the satellite altitude and the sheath resistance of the antenna. Each sample used in this wake study consisted of a case where one of the spheres was within ±30° of the anti-velocity vector direction. A total of 445 such cases were investigated and the results are summarized in Table 1. Unfortunately most of the wake effects observed with Injun 5 are not nearly as symmetrical and clearly defined as those shown in Figure 4 and in many cases it is not possible to clearly distinguish wake effects from other phenomena. In this study, any electric field perturbation which appeared to correlate even roughly with the angle between the sphere and the anti-velocity vector was classified as a wake, even though in some cases the perturbation may have been due to some other cause. The normalized frequencies of occurrence for wakes given in Table 1 show that the occurrence of wakes is a strong function of both altitude and sheath resistance. At altitudes below 1500 km and sheath resistances less than 10^5 ohms, the occurrence of wakes is negligibly small (1 case). At altitudes above 1500 km the occurrence of wakes is strongly controlled by the sheath resistance. For sheath resistances from 10^5 to 10^6 ohms only 8% of the cases investigated have wakes, whereas

for sheath resistances above 10^6 ohms 62% of the cases investigated have wakes. A qualitative comparison with the AFCRL electron density probe on Injun 5 indicates that wake effects are observed only in regions of very low electron density, typically 2×10^3 electrons/cm^3. In almost all cases investigated (88%) the potential of the sphere increased as the sphere passed through the wake region.

An unusual asymmetry exists between the +y and -y spheres in that wake effects are much more commonly observed with the +y sphere. In Figure 4 for example, no comparable perturbation of the -y sphere potential was observed even though the -y sphere passed through the wake region only a few minutes before the +y sphere. After normalization to account for the number of times each sphere was within the wake region, it was found that 70% of all wakes observed occurred for the +y sphere. The origin of this asymmetry is discussed below.

Discussion. The observed potential change as the sphere passes through the wake could be due either to the variation of the plasma potential in the wake region or to a perturbation in the sheath potential V_s. Several factors suggest that the increase in the sphere potential in the wake region is primarily due to a perturbation in the sheath potential. First, the fact that the wake occurrence is different for the two spheres indicates that the sphere potential perturbation in the wake depends on some parameter

which is different for the two spheres, rather than on a variation of the plasma potential in the wake region which should be the same for both spheres. Second, the observed positive potential in the wake region is not consistent with present theoretical understanding of spacecraft wakes [Al'pert et al., 1963; Taylor, 1967] in that the plasma potential in the wake region is expected to be negative in order to maintain approximate charge neutrality in this region of rarified ion density.

Within the wake region, the primary variation in the parameters affecting the sheath potential, V_s, is the decrease in the electron current, I_e, and the ion ram current, I_i, caused by the density rarefaction in the wake. For the high altitude, low density conditions where wake effects are observed, the ion ram current is negligible compared to either I_p or I_e. The increase in the sphere potential within the wake region can be caused by the decrease in the electron current, I_e, in the wake, for either a positive ion sheath [Equation (2)] or a photo-sheath [Equation (4)]. The pronounced asymmetry in the occurrence of wakes for the two spheres is believed to be caused by an asymmetry in the photo-electron emission from the two spheres caused, perhaps, by surface contamination during launch. The existence of a photo-electron current asymmetry of $I_{p+} - I_{p-} \simeq 1$ μamp is indicated by the jump in sphere potential that occurs regularly when the

spacecraft enters or leaves the earth's shadow. If the plasma sheath is a positive ion sheath for both spheres, then the dependence of the sheath potential on number density is the same for each sphere and wake effects will occur equally for each sphere, which is not what is generally observed. If, however, the density in the wake region becomes so low that a photo-sheath can occur, then a photo-sheath will form at a larger electron density for the +y sphere than for the -y sphere because of the asymmetrical photo-currents of the two spheres. It is therefore more likely for a photo-sheath to occur for the +y sphere than for the -y sphere. Also, since the photo-electron energy, U_p=1.5 volts, is much larger than the electron thermal energy, U_e≈0.1 volts, density-induced changes in the floating potential are much larger for a photo-sheath than for a positive ion sheath. Therefore, when a photo-sheath does develop for the +y sphere as it passes through the wake, the resulting perturbation in the sphere potential will be much larger than when both spheres have positive ion sheaths in the wake region.

From this analysis, it is concluded that the sphere potential perturbations observed in the wake region with Injun 5 occur when the sphere develops a photo-electron sheath in the region of reduced electron density in the

spacecraft wake. This interpretation is also consistent with the large ($>10^6$ ohms) sheath resistances observed when wake effects are observed since the resistance of a photo-sheath is much greater than the resistance of a positive ion sheath (compare Equations (1) and (3) when $U_p >> U_e$). It also explains why wake effects are observed only under conditions of very low density ($\sim 2 \times 10^3$ electrons/cm^3) since the photo-electron current must exceed the random electron current collected from the plasma (plus any amplifier current) in order for a photo-electron sheath to occur.

IV. DATA REDUCTION PROCEDURE

A. Residual Electric Field Determination

In order to separate naturally occurring electric fields from instrumental effects, it is necessary to subtract the $\vec{V}_s x \vec{B}$ electric field and other known errors from the measured electric field. The procedure used to eliminate the unwanted effects is described below.

All electric field effects are disregarded when the sheath resistance exceeds 10^6 ohms. This condition eliminates nearly all wake effects and assures that the differential amplifier impedance is much larger than the sheath resistance. Since spacecraft shadow effects are predictable from the spacecraft orientation, data are also discarded when a probe is close to the anti-sun vector. The component of the $\vec{V}_s x \vec{B}$ electric field parallel to the antenna axis, $\hat{y} \cdot \vec{V}_s x \vec{B}$, is also easily calculated. The only major problem which remains is boom shadowing. While boom shadowing is understood in principle, in practice this error cannot be calculated with sufficient accuracy to be useful because of uncertainties in the various plasma parameters involved.

The procedure which has been adopted for subtracting $\hat{y}\cdot\vec{V}_s x\vec{B}$ and the boom shadowing error is the following: a smooth curve E_s is hand-drawn through the measured electric field subject to the following requirements:

(1) It has a sine wave shape which is qualitatively the same as the computed $\hat{y}\cdot\vec{V}_s x\vec{B}$ field.

(2) The modulation amplitude and phase are adjusted to provide a good fit at low latitudes where no convection electric fields are expected.

(3) In cases of uncertainty the curve is drawn closer to the average measured field.

This procedure takes into account both $\hat{y}\cdot\vec{V}_s x\vec{B}$ and smooth changes in boom shadowing. In cases of uncertainty the residual electric field, $E_R=E_M-E_S$, will in general <u>underestimate</u> the actual convection electric field. If natural electric fields occur which are small and uniform over distances on the order of 5000 km, they will unfortunately but unavoidably be subtracted out by this procedure and will not appear in E_R. Because of the unknown spatial variations in the plasma parameters affecting the boom shadowing the absolute values of E_S and E_R cannot in general be determined to better than about $\pm$30 mV/meter. However, fluctuations in the residual electric field which occur with periods much less than the satellite spin period are considered significant if their magnitude exceeds about 10 mV/meter.

B. Convection Velocity Determination

Axford [1969] has explained that at Injun 5 altitudes the conductivities are such that a DC electric field is related to the convection velocity $\vec{V}_c$ of the plasma by the equation

$$\vec{V}_c = \frac{\vec{E}x\vec{B}}{B^2} . \tag{7}$$

The magnetic orientation of Injun 5 restricts the DC electric field experiment to measure only electric fields perpendicular to the geomagnetic field. Furthermore, since only the E_y component of the electric field is sensed, only the component of convection velocity parallel to the $\hat{z}$ axis of the spacecraft can be inferred. The convection velocity component measured can therefore be computed from the relation

$$\vec{V}_c = \frac{(E_R\hat{y})x(B\hat{z})}{B^2} = - \frac{E_R}{B}\hat{z} . \tag{8}$$

Figure 5 illustrates the data reduction procedure used to determine the residual electric field, E_R, for a typical case. The solid curve is the measured electric field, E_M, and the dotted curve, E_S, is the smooth curve drawn to best approximate the $\vec{V}_s x\vec{B}$ field and the boom shadowing error. The residual electric field, $E_R=E_M-E_S$, has an abrupt reversal of approximately $\pm$50 mV/meter at 1428 UT. The sheath impedance is

less than 10^6 ohms. The angles between the probes and the sun vector, θ_s, and between the probes and the satellite velocity vector, θ_v, verify that for this event neither probe was in a wake or a shadow. Hence, this electric field reversal is assumed to be due to a convection electric field.

The convection velocity component associated with this residual electric field is illustrated on a magnetic local time/invariant latitude polar diagram in Figure 6. Each arrow represents the measured component of the convection velocity computed using Equation (8). The length of the arrow is proportional to the magnitude of V_c and the direction of the arrow is in the direction of the convection velocity sensed. The base of each arrow, or the location of each dot, gives the satellite position at half-minute intervals. Since variations in V_c may occur within the 30 seconds between arrows, each arrow corresponds to the maximum or "envelope" convection velocity during the interval. It must be emphasized that the arrow represents only the component of the convection velocity detected; it does not represent the vector direction of the convection velocity since only one component is measured. The electric field reversal shown in Figure 5 appears in Figure 6 as a reversal in the east-west component of the convection velocity. Because of the orientation of the spacecraft during this event, the north-south component of the convection velocity cannot be determined.

The magnitudes of convection velocity variations determined on distance scales less than about 1000 km are believed to be uncertain by about 0.25 km/sec using this data reduction procedure and, as in the case of E_R, represent a lower limit. Uniform convection velocities over large regions (5000 km or greater) are not expected to be detectable if the convection velocity is less than about 1 km/sec because slowly-varying electric fields are eliminated in the data reduction procedure.

V. CHARACTERISTICS OF THE OBSERVED ELECTRIC FIELDS

On virtually every orbit of the satellite, significant residual electric fields not attributable to any known instrumental effect are observed. These electric field effects, which are assumed to be due to plasma convection phenomena, are only observed at middle and high latitudes. Above 60° invariant latitude, electric fields with fluctuations greater than 10 mV/meter are observed on nearly every pass and occasionally magnitudes greater than 100 mV/meter are observed. Many of these fluctuations take the form of discrete auroral zone events called electric field "reversals" discussed in section A below. Small changes sometimes observed at the plasmapause are discussed in Section B. Other electric field variations, irregular and broader in extent, are classified as "noise" and are discussed in Section C.

A. Auroral Zone Electric Field Reversals

A phenomenon which is observed to occur only in the auroral zone, but not on every pass, is an abrupt reversal in the residual electric field, E_R, and consequently, also in the convection velocity, V_c. These events are the easiest of the observed phenomena to study both because the signature of a reversal cannot arise due to a spurious shadow,

and also because the overall magnitude cannot be changed by an error in drawing E_s. Uncertainty is thus confined to where the electric field or convection velocity crosses zero; the peak-to-peak magnitude is unaffected by the data reduction.

An example of a reversal occurring at dusk at 78° INV has been shown in Figure 6. The convection direction, sunward at higher latitude, is observed less frequently than anti-sunward convection at higher latitudes, but both do occur. Figure 7 shows three reversals occurring at dawn on different days of January, 1969. The convection directions for the three are consistent in showing anti-sunward flow at higher latitudes, and sunward flow at lower latitudes. In all three examples the reversal occurs at about 75° INV. Reversals typically occur in the auroral zone between 70° and 80° INV and are not observed over the polar cap or at middle and low latitude.

Figure 8 shows a striking example of reversals which occur at conjugate ends of the same magnetic field lines. The polar diagrams represent opposite hemispheres 1 hour (one-half orbit) apart. On the dawn side, in the northern hemisphere, a reversal occurs at ∿74° INV. In the opposite hemisphere, the reversal occurs at 70° INV, again at ∿3.5 hours MLT. The convection velocities observed in association with this set of three reversals are among the largest ever observed with Injun 5. The electric fields (not shown) for these reversals

show several oscillations with ∿20 second periods on the low-latitude side of each of the three reversals. On the dusk side of Figure 8 another, smaller pair of conjugate reversals may be seen at 75° INV and ∿15.5 hours MLT.

Special mention should be made of the observation at 1643 UT in Figure 8. Here, because the satellite rotates, only the north-south component of convection is being measured. Simultaneously, the magnitude of convection measured becomes equal to zero, and afterwards again becomes non-zero. Both before and after, the convection is determined to have eastward components. This event is interpreted to mean that the true convection direction was eastward, with no north-south component. One hour later (at 1730 UT) at the magnetically conjugate location, only the east-west component was being measured, and large eastward convection is observed.

Figure 9 depicts an example of pairs of convection reversals occurring on both sides of the polar cap at about 75° INV, for three successive passes over the north polar cap. A large zone of convection appears to be directed across the center of the polar cap from ∿10:00 towards ∿22:00 hours MLT in the top diagram. At 1930 UT in the middle diagram the 04:00-16:00 hours MLT component of convection is being measured, and no electric field is measured. This does not rule out the

possibility that convection in the 10:00-22:00 direction persisted at 1930 UT. Some of the variation in velocity magnitude between passes in Figure 9 may be ascribed to the different orientations of the satellite. However, a close examination, for instance of the convection zones at 1924 and 2121 UT, shows that in the 2 hours between passes the magnitude of the eastward convection component changes significantly, the width of the zone changes, and the invariant latitude of the reversal shifts by several degrees. Thus the time scales of the phenomena in this example are shorter than the two hours between passes, although the overall pattern persists.

The convection shown in Figures 7, 8, and 9 may be summarized as illustrating the persistent occurrence of reversals in the east-west direction of the convection in the auroral zone. In most of these cases the primary convection pattern is limited to a region several degrees in latitude on either side of the reversal with sunward convection generally observed on the low latitude side of the reversal and anti-sunward convection on the high latitude side of the reversal. Insufficient data have been examined to determine to what extent a broad anti-sunward convection zone acorss the polar cap may occur, but broad convection zones with velocities as high as 2 km/sec over the polar region, such as those evident at 1727 UT in Figure 9, are definitely not common.

While not enough data has been studied to determine the dependence of the occurrence of reversals on magnetic activity, it is interesting to note that the examples of reversals shown in Figures 6, 7, 8, and 11 occurred when magnetic activity as measured by K_p was relatively quiet.

Reversals are abrupt boundaries between oppositely-directed electric field or convection "zones". Figure 10 shows two oppositely-directed electric field zones separated by a region of zero electric field, rather than by a sharp reversal. This pass is also of interest because the satellite was not rotating, and the electric antenna axis was parallel to the velocity vector, as illustrated in Figure 11. The orientation is fortunately such as to exclude all shadow and boom effects. Under this (rather rare) set of circumstances the potential across the polar cap may be integrated directly from the electric field:

$$\phi = - \int \vec{E} \cdot d\vec{s} \,. \qquad (9)$$

The potential, plotted in the top of Figure 10, reaches 44,000 volts in about 2500 kilometers. The polar diagram in Figure 11 shows the convection velocity components implied by the measured electric field zones. Only the sunward/anti-

sunward convection component is measured. The anti-sunward flow above 75° INV and sunward flow below 75° INV is consistent with the convection directions shown in Figures 7, 8, and 9.

Not all electric field reversals occur on time scales of minutes. Figure 12 shows a reversal which changes from minimum to maximum (117 mV/meter) in 8 seconds. As the $\hat{y}$ axis at this time was aligned parallel to $\vec{V}_s$, the potential may again be found as indicated by Equation (9). The top of Figure 12 shows the potential obtained, which reaches 3600 volts in less than 100 km.

B. The Plasmapause Boundary

Several plasmapause crossings have been investigated to determine if any changes occur in the plasma convection velocity as the satellite crosses the plasmapause/light ion trough boundary [Carpenter, 1966; Taylor et al., 1969]. The plasmapause boundary can be identified in the Injun 5 data from (1) the characteristic "lower hybrid resonance (LHR) breakup" effect commonly found in the VLF electric field data at the plasmapause boundary [Carpenter et al., 1968], (2) the characteristic increase in the sheath resistance at the plasmapause boundary and (3) the change in the electron density as measured directly by the AFCRL electron density measurement on Injun 5. Unfortunately, for the Injun 5 orbit these plasmapause indicators are not always present so that a unique

identification of the plasmapause location is possible for only a small fraction of the available data, primarily at altitudes above 2000 km during local night. Because of these limitations only eight cases have been investigated at the present time for which the plasmapause location can be clearly and unambiguously identified. Of these eight cases five have small (10-20 mV/meter), but clearly distinguishable perturbations in the residual electric field at the plasmapause boundary.

An illustration of one such plasmapause crossing is shown in Figure 13. In this case the plasmapause crossing, from the plasmasphere into the trough region, occurred at about 0806:15 ±:15 UT, as shown by the increase in sheath resistance at this time. The DC electric field varies smoothly as the satellite crosses the plasmapause, with no evidence of the large amplitude electric field variations observed at higher latitudes. A small shift in the DC electric field is evident, however, shortly after crossing the plasmapause boundary. In this case, the antenna axis is aligned north-south so that the east-west component of the convection velocity is being detected. By extrapolating the $\vec{V}_s x \vec{B}$ electric field into the trough region (dotted line in Figure 13) the convection electric field in the region beyond the plasmapause boundary the convection electric field can be estimated to be about 15 mV/meter. This electric field

corresponds to a westward convection velocity of about 0.5 km/sec on the high latitude side of the plasmapause boundary.

All of the five plasmapause crossings observed with significant electric field effects at the boundary occurred in the local time range from 0 to 5 hours magnetic local time. The direction of the convection velocity component measured in these five cases was as follows: three cases west, one case north-west, and one case south. The magnitude of the change in electric field detected in all of these cases was small, 10 to 20 mV/meter, and close to the resolution limit of the instrument and the data analysis technique used.

Discussion. The possibility that these small perturbations in the DC electric field near the plasmapause boundary could be caused by a change in the sheath characteristics rather than a real electric field has been investigated in some detail. Two possibilities have been considered: (1) errors caused by the change in the sheath resistance, and (2) errors caused by an imbalance in the parameters affecting the sheath voltages of the two spheres. In none of the cases investigated was the change in the sheath resistance large enough to produce the observed effect. The possible quantities which could contribute to an imbalance of the two sheath voltages can be seen from Equation (2). Because the electron thermal velocity greatly exceeds the spacecraft velocity the terms U_e and I_e in Equation (2) are always the same for the two

spheres and cannot cause a difference in the sheath voltages. The ion ram current I_i, which is directly proportional to the plasma density, changes considerably at the plasmapause. An inequality of either of the terms, I_i or I_p in Equation (2) could cause a change in the differential sheath voltage at the plasmapause. However, since I_i is much less than I_p at the altitude where these events were observed, the effect of changing I_i is quite small, less than 3 mV/meter for almost any reasonable condition. Furthermore, in two of the plasmapause cases studied [Figure 13 of this paper and Figure 4 of Gurnett, 1970] the spacecraft orientation was such that neither sunlight nor ram ion shadowing by the booms was possible so that the sheath voltages should be identical for the two spheres. Since no other instrumental effect is known which could account for the observed potential changes, it is concluded that these plasmapause electric field effects are due to a change in the plasma convection at the plasmapause boundary.

C. High-latitude Electric Field Noise

At invariant latitudes greater than 60° electric field "noise" is nearly always observed. This noise consists of rapid fluctuations of the observed electric field, with time scales generally less than 60 seconds and amplitudes up to 150 mV/meter. An example of this type of electric field noise is illustrated in Figure 14. Some of the general characteristics of this electric field noise are summarized

below:

(1) There is an apparent seasonal effect, with larger noise amplitudes occurring over the winter polar region, as evident in the example shown in Figure 14.

(2) The noise usually has a fairly well-defined low-latitude limit at about 58° to 62° invariant latitude. When the amplitude of the noise is very low, however, the noise may not be observable below about 70° invariant latitude.

(3) When the noise amplitudes are very low, the invariant latitude at which the fluctuations are largest is nearly always at about 70 to 75° invariant latitude, in the auroral zone.

(4) The amplitude of the noise is strongly dependent on altitude with larger noise levels observed at higher altitudes.

(5) The amplitude of the noise is also related to the sheath resistance, to the extent that when $R_s < 10^6$ ohms, fluctuations rarely exceed 50 mV/meter, and are more typically 10 mV/meter in amplitude, whereas when $R_s > 10^6$ ohms, the noise amplitudes may exceed 150 mV/meter, but are more typically about 30 mV/meter in amplitude.

(6) The noise amplitude is also related to the electron density in that the large noise levels are generally observed in regions of low electron density.

Because of the interdependence of the electron density, sheath resistance, season, satellite position, and possibly other factors, it is difficult to determine which factors are most significant in controlling the noise amplitude. Since spacecraft wake effects also occur at high latitudes and high sheath resistances, large electric field fluctuations are usually observed superimposed on the sphere potential perturbations due to the spacecraft wake. The noise does not, however, appear to be related to the spacecraft wake effect because the noise is present with essentially the same amplitude both when the sphere is inside and when it is outside the wake region. An initial comparison of noise amplitudes during two magnetically disturbed and two magnetically quiet times in January, 1969, reveals no significant correlation with magnetic activity.

Discussion. The DC electric field noise may well be due to magnetospheric convection; possibly small-scale eddies or turbulence. If so, then the altitude dependence of the noise amplitude provides evidence for DC electric fields parallel to the geomagnetic field. Because the noise amplitudes are typically 30 mV/meter, or more, at apogee, but

are usually negligible by comparison at perigee over the same region, then there must be a potential drop on the order of 30 mV/meter x (typical scale length $\simeq$ 30 km) = 900 volts between apogee (2528 km) and perigee (677 km). A lower limit on the corresponding parallel electric field would therefore be about 0.5 mV/meter.

It is, however, also possible that this "electric" field noise may be due to unbalanced variations of the sheath potential or to some other unknown interaction between the spacecraft and the surrounding medium. Unbalanced fluctuations in the sheath potentials could be caused by spatial variations in the plasma parameters (primarily electron density and temperature) if a suitable bias asymmetry exists for the two spheres. The most likely parameter which could cause these potential variations is believed to be the electron temperature, since the sheath potential [Equation (2)] is directly proportional to the electron temperature whereas the electron density enters only in the logarithmic term.

Although unbalanced fluctuations in the sheath potentials may provide a possible qualitative explanation of the high-latitude electric field noise, an initial investigation does not indicate that this process is occurring. In particular, (1) a detailed comparison of the electric field noise with data from the AFCRL experiment on Injun 5, which measures a quantity proportional to $N_e\sqrt{T_e}$, reveals no

significant correlation, and (2) a comparison of the electric field noise fluctuations with sheath resistance variations (R_s in Equation (1) is proportional to T_e, but is measured only every 30 seconds) also reveals no consistent correlation on the time scale being considered. At this time it has not, therefore, been possible to identify this high-latitude electric field noise with any known sheath effect or interaction of the spacecraft with the surrounding medium.

VI. CONCLUSIONS

A. Summary of Observations

Electric field reversals are the most significant convection electric field effect identified in the Injun 5 DC electric field data. Electric field reversals consistently occur on both the dawn and dusk sides of the polar cap at about 70° to 80° invariant latitude, and have been identified at magnetically conjugate points in both hemispheres. Amplitudes of 30 mV/meter, and occasionally greater than 100 mV/meter, occur frequently. The detailed location and form of the reversal often changes markedly on time scales less than 2 hours. Generally the plasma convection velocities associated with reversals on the dawn-dusk meridian are antisunward at higher latitudes and sunward at lower latitudes, but cases of convection directions opposite to this do occur. Over the polar region above the auroral zone the convection velocity is usually small compared to the convection velocities in the region of the reversal.

Small changes in the DC electric field, typically 10 to 20 mV/meter, sometimes occur at the plasmapause/light ion trough boundary. For the cases investigated, all of which were at magnetic local times from 0 to 5 hours, the convection

observed generally has a westward component on the high-latitude side of the plasmapause boundary, relative to a coordinate system co-rotating with the earth.

Noise-like electric field fluctuations with time scales less than 60 seconds and amplitudes of 10 mV/meter or greater are usually observed at high latitudes. The low-latitude boundary of this noise is typically at about 60° invariant latitude. The amplitude of this noise increases significantly with increasing altitude and is largest at high altitudes over the winter hemisphere. This altitude dependence implies the presence of significant electric fields parallel to the geomagnetic field. However, some possibility exists that these noise-like electric field fluctuations may not be due to real magnetospheric electric fields, but may be caused by unbalanced variations in the sheath potential or some other yet unknown interaction between the spacecraft and the surrounding medium.

B. Comparison with Barium Cloud Measurements

Haerendel and Lüst [1970] summarize recent results of measurements of plasma convection by the barium cloud drift technique. The requirement of twilight conditions restricts barium cloud measurements to the midnight sector and invariant latitudes generally below 70°. However, at local times nearer dawn, eastward drifts are observed, and near dusk, westward

drifts. These directions are entirely consistent with the "sunward" convection reported in this paper at dawn and dusk at comparable latitudes. Several cases of clouds reversing their drift directions have been reported. Furthermore, the magnitudes of convection velocities we observe are consistent with, for instance, those quoted by Wescott et al., [1969], who report intensities of 10 - 130 mV/meter. These authors also report that large irregularities in the electric field exist most of the time.

C. Comparison with Magnetospheric Models

Dungey [1961] suggested that the solar magnetic field could merge with the earth's magnetic field in an "open" magnetospheric model. Field lines merged at the bow of the magnetosphere would be pulled across the polar caps by the solar wind and would reconnect on the earth's night side. Consequently there would be a return flow of field lines to the sunward side of the earth at lower latitudes. As charged particles would remain attached ("frozen") to field lines except near reconnection regions, bulk motion, or convection, of the magnetosphere would result. The measurements presented here of DC electric fields related directly to plasma convection, indicate that the anti-solar convection flow across the polar caps suggested by Dungey is not a normal feature of the magnetosphere. Figures 9 and 11 suggest that such a convective flow may occasionally occur,

but the velocities are less than would be expected from a geometrical reduction of the solar wind velocity to satellite altitudes.

Axford and Hines' [1961] "closed" magnetospheric model more explicitly suggested convection across the polar cap with return flow at the auroral zone, but used "viscous interaction" with the solar wind at the magnetospheric boundary as the principal driving force. To the extent that their trans-polar flow was concentrated at auroral zone latitudes, the observations presented herein are consistent with the Axford and Hines model. However, we do not observe large-scale convection directly across the polar cap to be an ordinary feature of magnetospheric convection.

The small-scale westward convection observed just outside the plasmapause boundary is consistent in magnitude and direction with the interpretation that the plasmapause may be the boundary of the plasma which corotates with the earth. (The frame of reference used <u>is</u> corotating with the earth.)

D. <u>Comparison with Models of Substorms and Aurorae</u>

The short time scales we observe for major changes in the magnetospheric electric fields measured, suggest ties with magnetic substorm phenomena. The same essential features of high latitude convection, anti-sunward trans-polar flow

and auroral zone return paths, appear in the magnetic substorm equivalent current systems derived by Nishida [1967], Heppner [1969], Wescott et al., [1969], and others, on the basis of ground magnetometer measurements. These currents are assumed to be concentrated in the ionosphere. The principal point of disagreement of our observations with the pattern is again that we observe the anti-solar convection generally to be concentrated in the auroral zone, rather than spread out across the polar cap. However, as we do occasionally (cf. Figures 9 and 11) see trans-polar flow components, and since the substorm current pattern is presumably a transitory feature of the ionosphere, we cannot reject the possibility of its validity.

A competing theory of magnetic substorms utilizes a 3-dimensional current system with field aligned currents [Boström, 1967; Bonnevier, et al., 1970, Akasofu and Meng, 1969]. A current is assumed to flow through the ionosphere (auroral electrojet) from dawn to dusk, then outward along a dusk magnetic field line. There the ring current, which drives the system, connects dusk to dawn, where the current flows inward along a field line. The effects of such field-aligned currents in the ionosphere have been investigated theoretically by Block and Fälthammar [1968], leading to a theory of space-charge regions above aurorae [Carlqvist and Boström, 1970]. One of the consequences of such a space-charge region is the existence of a current slab above the aurora

containing a north-south electric field which reverses in the center of the slab. The fields will point towards the center if the field-aligned current is upwards, and away from the slab center if the field aligned current is downwards. The electric fields are then presumed to cause $\vec{E}x\vec{B}/B^2$ drifts. With the current system postulated, these drifts will be sunwards at latitudes below the aurora and anti-sunward at higher latitudes. These fields and drifts are entirely consistent with our observations of the predominant directions of reversals. Carlqvist and Boström predict potentials at the center of the slabs of 10^3-10^5 volts, and this is consistent with the 3600 volt and 44,000 volt examples shown in Figures 10 and 12. If one assumes slab widths of 10^2-10^3 kilometers, the range of convection velocities predicted also encompasses the range of velocities observed.

ACKNOWLEDGMENTS

The authors would like to thank Dr. R. Sagalyn for providing electron number density data from the AFCRL experiment on Injun 5.

This research was supported in part by the National Aeronautics and Space Administration under contracts NAS5-10625, NAS1-8141, NAS1-8144(f), NAS1-8150(f), and NGL-16-001-043(97); and by the Office of Naval Research under contract N00014-68-A-0196-0003.

REFERENCES

Aggson, T., A proposal for tri-axial electric field measurements on IMP spacecraft H, I, and J, NASA-Goddard Space Flight Center preprint, October 1966.

Akasofu, S. I., and C. I. Meng, A study of solar magnetic substorms, J. Geophys. Res., 74 (1), 293-313, January 1969.

Al'pert, Ja. L., A. V. Gurevic, and L. P. Pitaevskij, Effects due to an artificial earth satellite in rapid motion through the ionosphere or the interplanetary medium, Space Science Reviews, 2, 680-748, 1963.

Axford, W. I., Magnetospheric convection, Reviews of Geophys., 7, 421-459, 1969.

Axford, W. I., and C. O. Hines, A unifying theory of high-latitude geophysical phenomena and geomagnetic storms, Can. J. Phys., 39, 1433, 1961.

Block, L. P., and C.-G. Fälthammar, Effects of field-aligned currents on the structure of the ionosphere, J. Geophys. Res., 73 (15), 4807-4812, August 1968.

Bonnevier, B., R. Boström, and G. Rostocker, A three-dimensional model current system for polar magnetic substorms, J. Geophys. Res., 75 (1), 107-122, January 1970.

Boström, R., Auroral electric fields, Aurora and Airglow, B. M. McCormac, ed., Reinhold Book Corp. (New York), 293-303, 1967.

Brace, L. H., B. M. Reddy, and H. G. Mayr, Global behavior of the ionosphere at 1000 kilometer altitude, J. Geophys. Res., 72, 265, 1967.

Cain, J. C., S. J. Hendricks, R. A. Langel, and V. W. Hudson, A proposed model for the international geomagnetic reference field -- 1965, J. Geomagn. Geoelec, 19, 335, 1967.

Carlqvist, P., and R. Boström, Space charge regions above the aurora, J. Geophys. Res., 75 (34), 7140-7146, December 1970.

Carpenter, D. L., Whistler studies of the plasmapause in the magnetosphere, 1, Temporal variations in the position of the knee and some evidence on plasma motion near the knee, J. Geophys. Res., 71 (3), 693-709, 1966.

Carpenter, D. L., Whistler evidence of the dynamic behavior of the duskside bulge in the plasmasphere, J. Geophys. Res., 75 (19), 3837-3847, July 1970.

Carpenter, D. L., F. Walter, R. E. Barrington, and D. J. McEwen, Alouette 1 and 2 observations of abrupt changes in whistler rate and of VLF noise variations at the plasmapause: A satellite-ground study, J. Geophys. Res., 73, 2929, 1968.

Dungey, J. W., Interplanetary magnetic field and the auroral zone, Phys. Rev. Letters, 6, 47-48, 1961.

Fahleson, U. V., Theory of electric field measurements conducted in the magnetosphere with electric probes, Space Sci. Rev., 7, 238, 1967.

Fahleson, U. V., M. C. Kelley, and F. S. Mozer, Investigation of the operation of a DC electric field detector, preprint, University of California, September 30, 1968.

Föppl, H., G. Haerendel, L. Haser, R. Lüst, F. Melzner, B. Meyer, H. Neuss, H. Rabben, E. Rieger, H. Stocker, and W. Stoffregen, Preliminary results of electric field measurements in the auroral zone, J. Geophys. Res., 73, 21-26, 1968.

Gurnett, D. A. Satellite measurements of DC electric fields in the ionosphere, Particles and Fields in the Magnetosphere, B. M. McCormac, ed., Reinhold Book Company, (Dordrecht, Holland) 239-246, 1970.

Gurnett, D. A., G. W. Pfeiffer, R. R. Anderson, S. R. Mosier, and D. P. Cauffman, Initial observations of VLF electric and magnetic fields with the Injun 5 satellite, J. Geophys. Res., 74 (19), 4631-4648, September 1969.

Haerendel, G., and R. Lüst, Electric fields in the ionosphere and magnetosphere, Particles and Fields in the Magnetosphere, B. M. McCormac, ed., Reinhold Book Company (Dordrecht, Holland) 213-228, 1970.

Haerendel, G., R. Lüst, and E. Reiger, Motion of artificial ion clouds in the upper atmosphere, Planetary Space Sci., 15, 1-18, 1967.

Heppner, J. P. Magnetospheric convection patterns inferred from high-latitude activity, Atmospheric Emissions, B. M. McCormac and A. Omholt, eds., Van Nostrand Reinhold Co. (New York) 251-266, 1969.

Heppner, J. P., T. L. Aggson, and N. C. Maynard, paper delivered at the Symposium on the Physics of the Magnetosphere (abstract), Washington, D. C., September 1968.

Maynard, N. C., and J. P. Heppner, Variations in electric fields from polar orbiting satellites, Particles and Fields in the Magnetosphere, B. M. McCormac, ed., Reinhold Book Company (Dordrecht, Holland) 247-253, 1970.

Mozer, F. S., and P. Bruston, Electric field measurements in the auroral ionosphere, J. Geophys. Res., 72 (3), 1109-1114, 1967.

Mozer, F. S., and R. Serlin, Magnetospheric electric field measurements with balloons, J. Geophys. Res., 74 (19), 4739-4754, September 1969.

Nishida, A., Average structure and storm-time change of the polar topside ionosphere at sunspot minimum, J. Geophys. Res., 72 (23), 6051-6061, December 1967.

Piddington, J. H., A hydromagnetic theory of geomagnetic storms and auroras, Planetary Space Sci., 9, 947-957, 1962.

Potter, W. E., Rocket measurements of auroral electric and magnetic fields, J. Geophys. Res., 75 (28), 5415-5431, October 1970.

Taylor, H. A., Jr., H. C. Brinton, D. L. Carpenter, F. M. Bonner, and R. L. Heyborne, Ion depletion in the high-latitude exosphere; simultaneous OGO 2 observations of the light ion trough and the VLF cutoff, J. Geophys. Res., 74 (14), 3517-3528, July 1969.

Taylor, J. C., Disturbance of a rarified plasma by a supersonic body on the basis of the Poisson-Vlasov Equations 1, Planetary and Space Sci., 15, 155, 1967.

Van Allen, J. A., On the electric field in the earth's distant magnetotail, J. Geophys. Res., 75 (1), 29-38, January 1970.

Wescott, E. M., J. D. Stolarik, and J. P. Heppner, Electric fields in the vicinity of auroral forms from motions of barium vapor releases, J. Geophys. Res., 74 (14), 3469-3487, 1969.

TABLE 1

Percent Occurrence of Wakes

Altitude (Kilometers)	Impedance (Ohms) $10^4 - 9 \times 10^5$	$10^5 - 9 \times 10^6$	$>10^6$
>2500	(0)	5% (22)	55% (11)
2000 - 2400	(0)	11% (27)	58% (52)
1500 - 1900	(0)	15% (106)	76% (21)
1000 - 1400	0% (2)	4% (119)	100% (1)
500 - 900	3% (31)	0% (53)	(0)
All Altitudes	3% (33)	8% (327)	62% (85)

Number in parentheses indicates number of samples

Total number of samples (probe within ±30° of $-\vec{V}_s$): 445

FIGURE CAPTIONS

Figure 1 Views of the Injun 5 satellite showing the electric antennas and their orientation after spacecraft alignment with the local geomagnetic field.

Figure 2 Top: Schematic illustration of the plasma sheath around the spacecraft and electric probes. Bottom: Equivalent circuit of the probe-plasma system.

Figure 3 Electric field $E = -\frac{V_+ - V_-}{\ell}$ measured for one full orbit of the Injun 5 spacecraft, compared with calculated values of $|\vec{V}_s \times \vec{B}|$. Variations in the resistance of the plasma sheath around the antennas are shown below.

Figure 4 Spacecraft wake effects observed on 3 successive high-altitude passes over the northern hemisphere in January, 1969.

Figure 5. Example of a sudden reversal in the convection electric field. E_M is the measured electric field; E_s is the $\vec{y} \cdot \vec{V}_s \times \vec{B}$ electric field; and $E_R = E_M - E_s$ is assumed to be the convection electric field. Antenna orientation angles and sheath impedance (see text) are used to verify that the reversal is not an instrumental effect.

Figure 6 Convection velocity components inferred from $\vec{v}_c = \vec{E}_R x \vec{B}/B^2$ for the electric field reversal shown in Figure 5. The arrow represents only the convection velocity component sensed and does not represent the vector direction of the convection velocity since only one component is measured.

Figure 7 Convection velocity reversals inferred from DC electric field measurements on three different days of January, 1969. The reversals occur at dawn and all have sunward (anti-sunward) components on the low (high) latitude side of the reversal.

Figure 8 Convection velocity reversals observed to occur on conjugate ends of the same geomagnetic field lines, one hour apart. The five reversals shown, three at 3:00 MLT and two at 15:00 MLT, all possess sunward (anti-sunward) convection components on the low (high) latitude sides of the reversals.

Figure 9 Pairs of convection velocity reversals observed at dawn and dusk MLT on three successive passes over the northern polar cap. The existence of a temporary anti-sunward convection zone across the polar cap is suggested by the data on the top figure.

Figure 10 Electric field measured parallel to the satellite path for a southern polar cap pass at low altitude. The potential $\phi = -\int \vec{E} \cdot d\vec{s}$ reaches 44,000 volts in 2500 kilometers.

Figure 11 Convection velocity components corresponding to the electric fields shown in Figure 10. The spacecraft orientation, as shown, is such that only the 1:00-13:00 MLT component is measured, since the satellite was not rotating for this pass. Sunlight shadows of the spacecraft body or booms on the spheres cannot occur for this orientation.

Figure 12 Example of a very rapid reversal in the north-south electric field. The potential $\phi = -\int \vec{E} \cdot d\vec{s}$ reaches 3600 volts in less than 100 kilometers.

Figure 13 Example of a small electric field change observed near the plasmapause/light ion trough boundary.

Figure 14 Example of electric field noise observed across the polar caps for a full orbit during January, 1969. The noise amplitudes are largest over the winter pole and at high altitudes where the sheath resistances are also large.

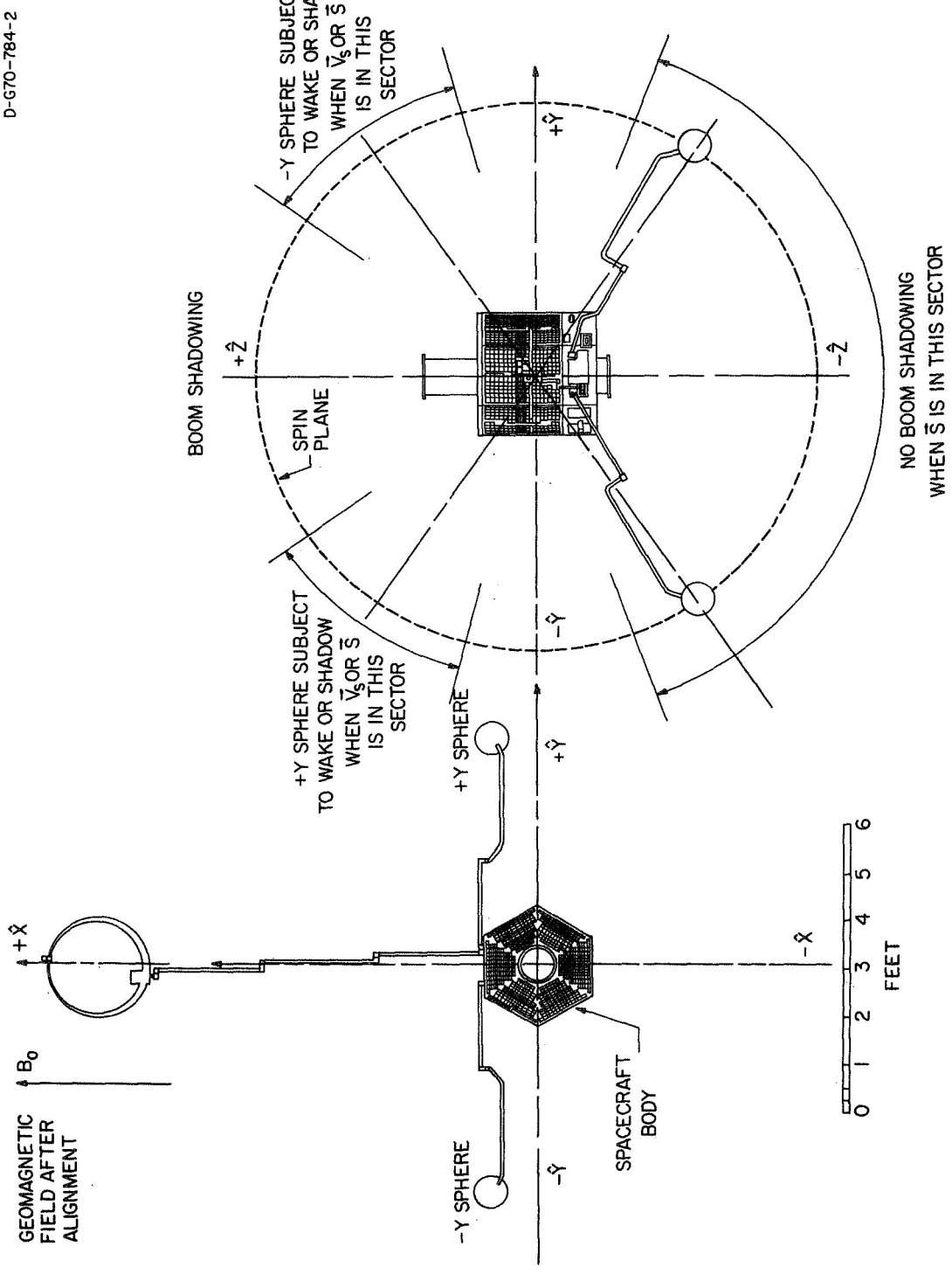
D-G70-784-2
GEOMAGNETIC FIELD AFTER ALIGNMENT
B_0
+X̂
-X̂
+Ŷ
-Ŷ
+Ẑ
-Ẑ
+Y SPHERE
-Y SPHERE
SPACECRAFT BODY
+Y SPHERE SUBJECT TO WAKE OR SHADOW WHEN $\vec{V}_s$ OR $\vec{S}$ IS IN THIS SECTOR
-Y SPHERE SUBJECT TO WAKE OR SHADOW WHEN $\vec{V}_s$ OR $\vec{S}$ IS IN THIS SECTOR
BOOM SHADOWING
SPIN PLANE
NO BOOM SHADOWING WHEN $\vec{S}$ IS IN THIS SECTOR
VIEW FROM -Z AXIS
VIEW FROM +X̂ AXIS
0 1 2 3 4 5 6
FEET

Figure 1

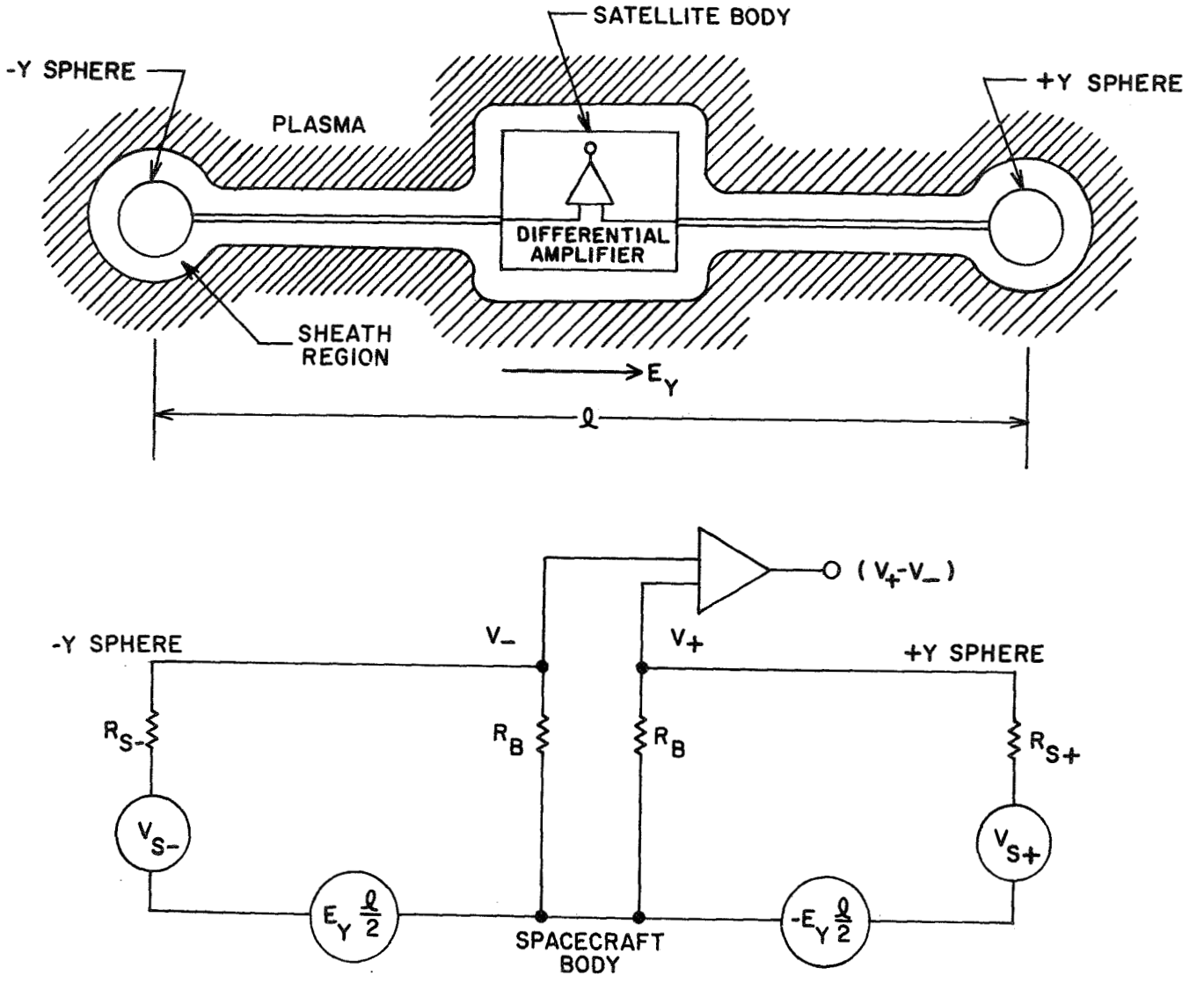
SATELLITE BODY
-Y SPHERE
+Y SPHERE
PLASMA
DIFFERENTIAL AMPLIFIER
SHEATH REGION
E_Y
ℓ
$(V_+ - V_-)$
-Y SPHERE
V_-
V_+
+Y SPHERE
R_{S-}
R_B
R_B
R_{S+}
V_{S-}
V_{S+}
$E_Y \frac{\ell}{2}$
$-E_Y \frac{\ell}{2}$
SPACECRAFT BODY

Figure 2

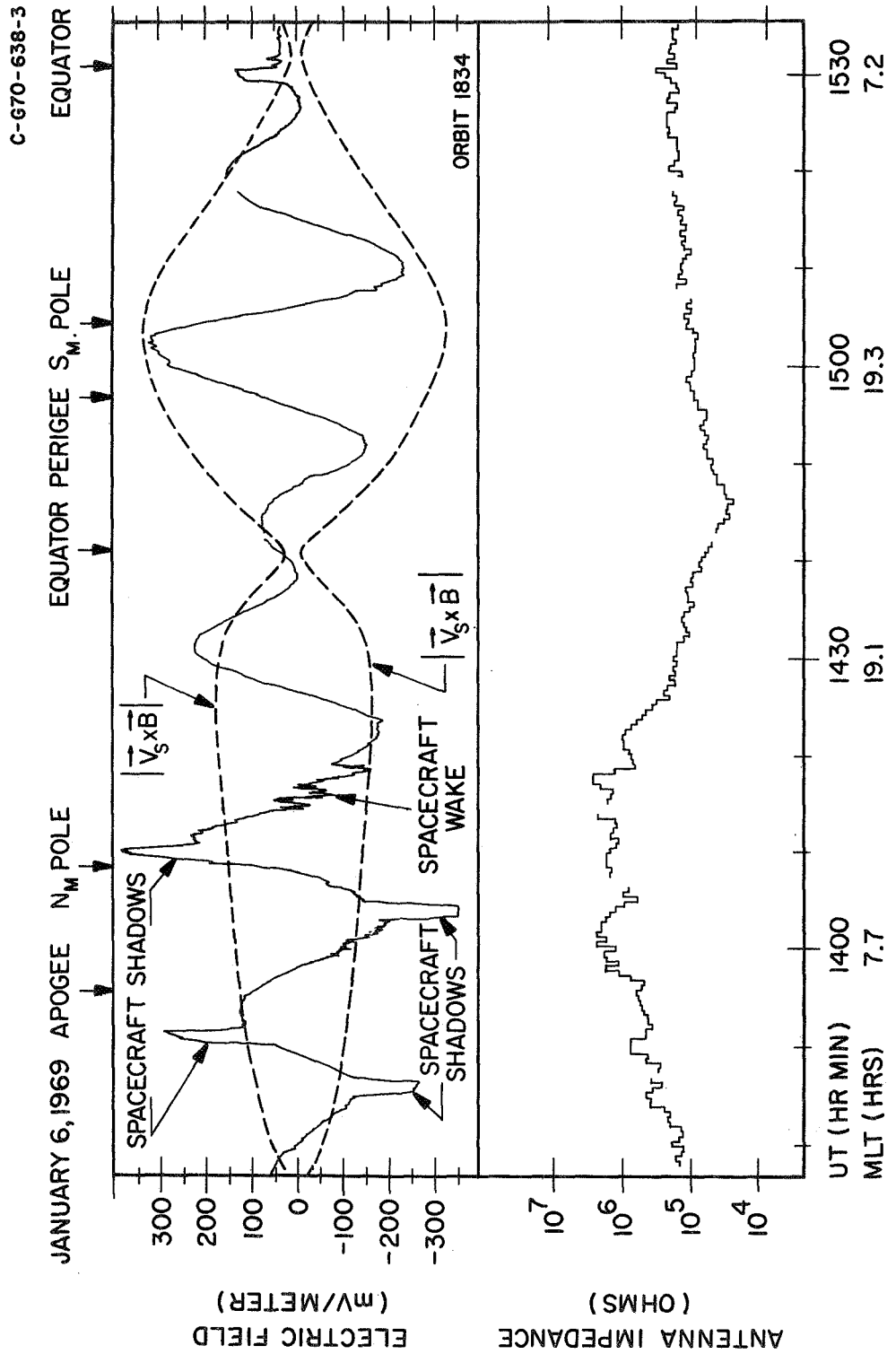
C-670-638-3
JANUARY 6, 1969 APOGEE N_M POLE
EQUATOR PERIGEE S_M POLE EQUATOR
ORBIT 1834
SPACECRAFT SHADOWS
$|\vec{V}_S \times \vec{B}|$
SPACECRAFT WAKE
SPACECRAFT SHADOWS
$|\vec{V}_S \times \vec{B}|$
ELECTRIC FIELD (mV/METER)
300
200
100
0
-100
-200
-300
ANTENNA IMPEDANCE (OHMS)
10^7
10^6
10^5
10^4
UT (HR MIN) 1400 1430 1500 1530
MLT (HRS) 7.7 19.1 19.3 7.2

Figure 3

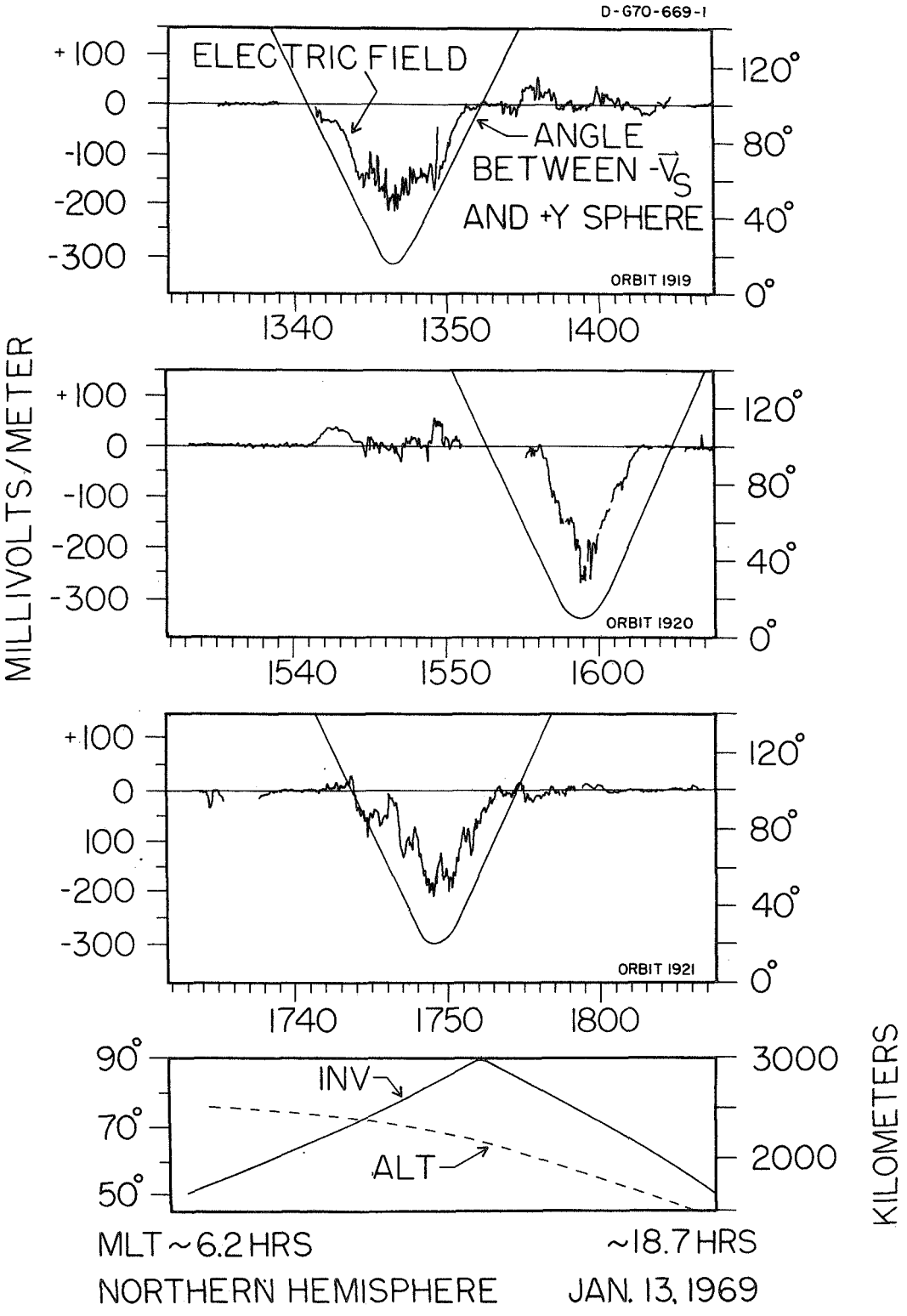
D-G70-669-1
ELECTRIC FIELD
ANGLE BETWEEN -$\vec{V}_S$ AND +Y SPHERE
ORBIT 1919
ORBIT 1920
ORBIT 1921
+100
0
-100
-200
-300
120°
80°
40°
0°
1340
1350
1400
1540
1550
1600
1740
1750
1800
MILLIVOLTS/METER
90°
70°
50°
INV
ALT
3000
2000
KILOMETERS
MLT ~ 6.2 HRS
~18.7 HRS
NORTHERN HEMISPHERE
JAN. 13, 1969

Figure 4

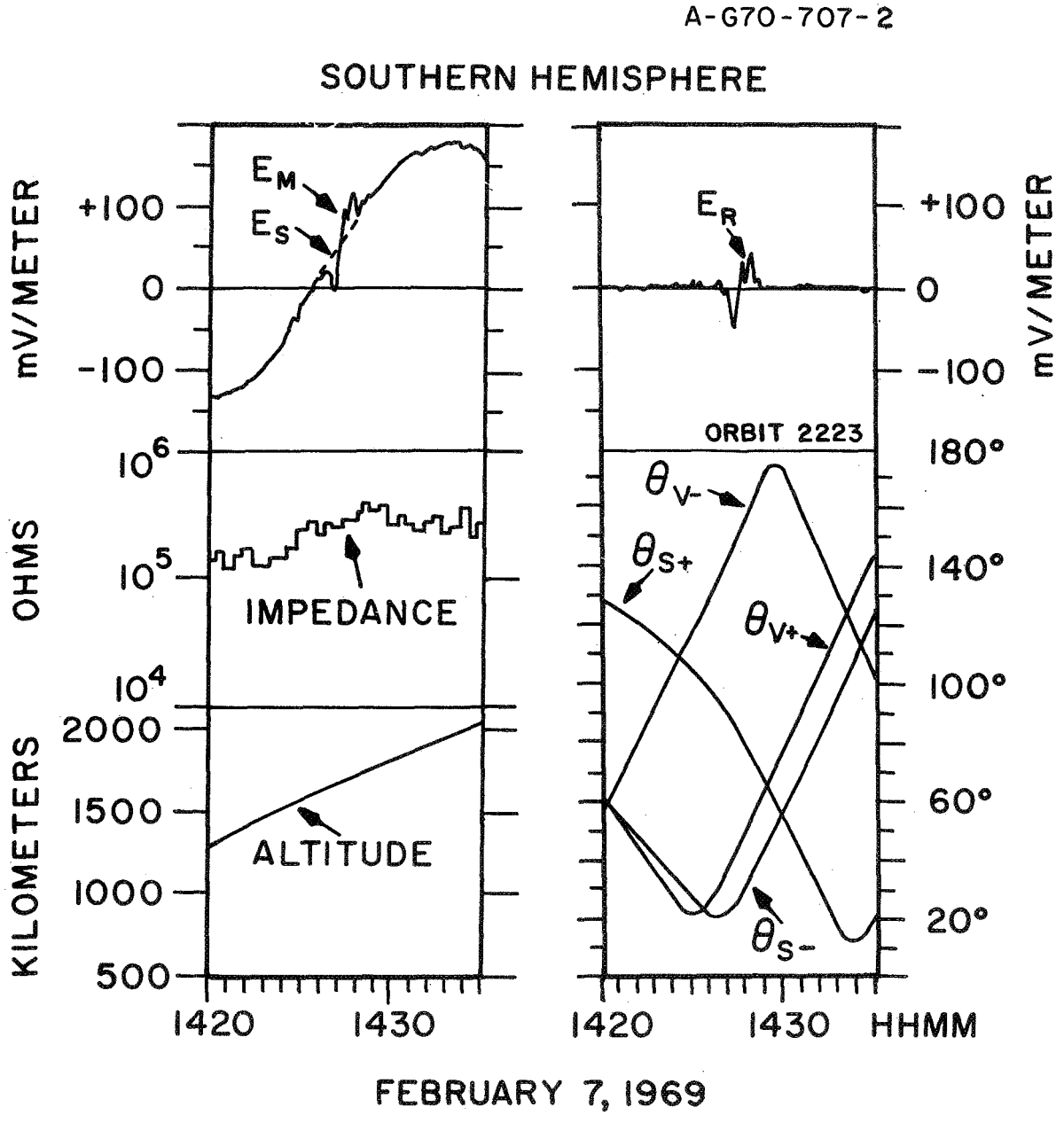
A-G70-707-2
SOUTHERN HEMISPHERE
mV/METER
+100
0
-100
E_M
E_S
E_R
ORBIT 2223
OHMS
10^6
10^5
10^4
IMPEDANCE
KILOMETERS
2000
1500
1000
500
ALTITUDE
θ_{V-}
θ_{S+}
θ_{V+}
θ_{S-}
180°
140°
100°
60°
20°
1420
1430
HHMM
FEBRUARY 7, 1969

Figure 5

A-G70-706-1

SOUTHERN HEMISPHERE
ORBIT 2223
K_p = 2+
K_p SUM = 16,M

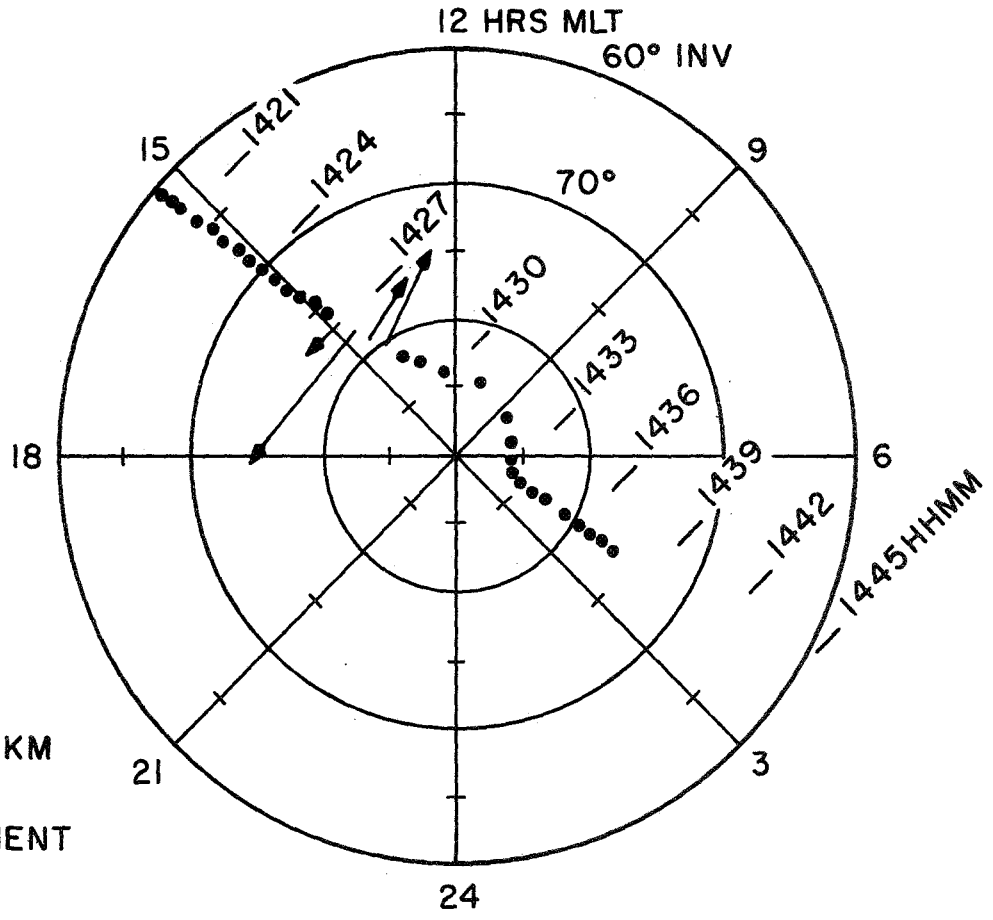

FEBRUARY 7, 1969
ALTITUDE AT REVERSAL~1700 KM

CONVECTION VELOCITY COMPONENT

1 KM/S

Figure 6

D-G70-673-1

ORBIT 1860
K_p = 2+
K_p SUM = 16-

SOUTHERN HEMISPHERE
JANUARY 8, 1969
ALTITUDE ~ 1200KM

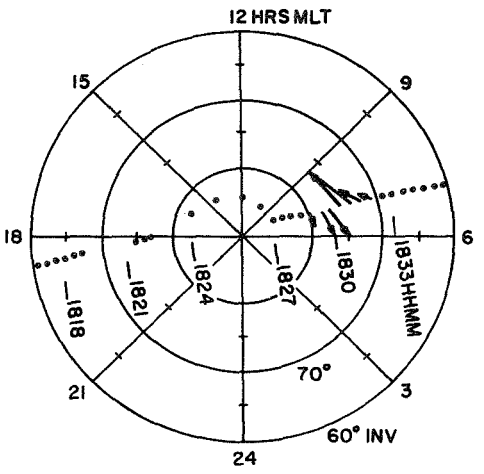

ORBIT 1884
K_p = 1-
K_p SUM = 6-

SOUTHERN HEMISPHERE
JANUARY 10, 1969
ALTITUDE ~ 1200KM

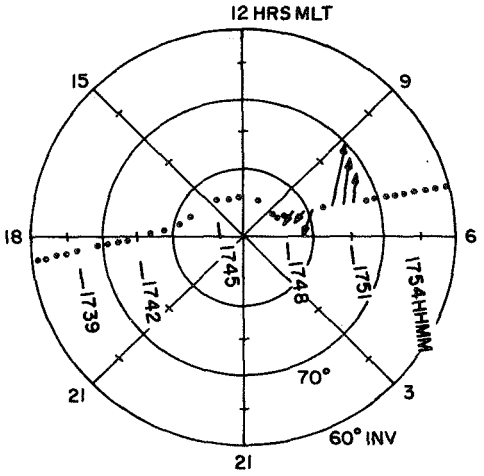

ORBIT 1980
K_p = 3-
K_p SUM = 27, D

SOUTHERN HEMISPHERE
JANUARY 18, 1969
ALTITUDE ~ 1300KM

CONVECTION VELOCITY COMPONENT
1 KM/S

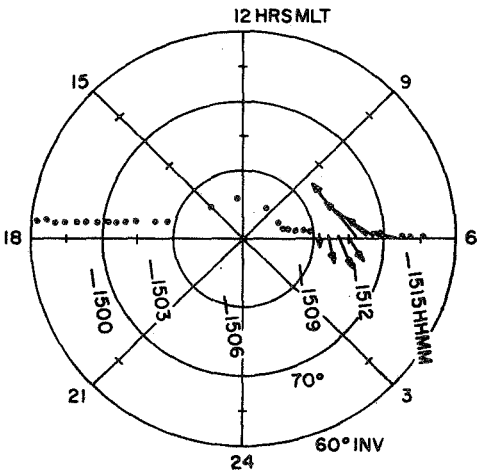

Figure 7

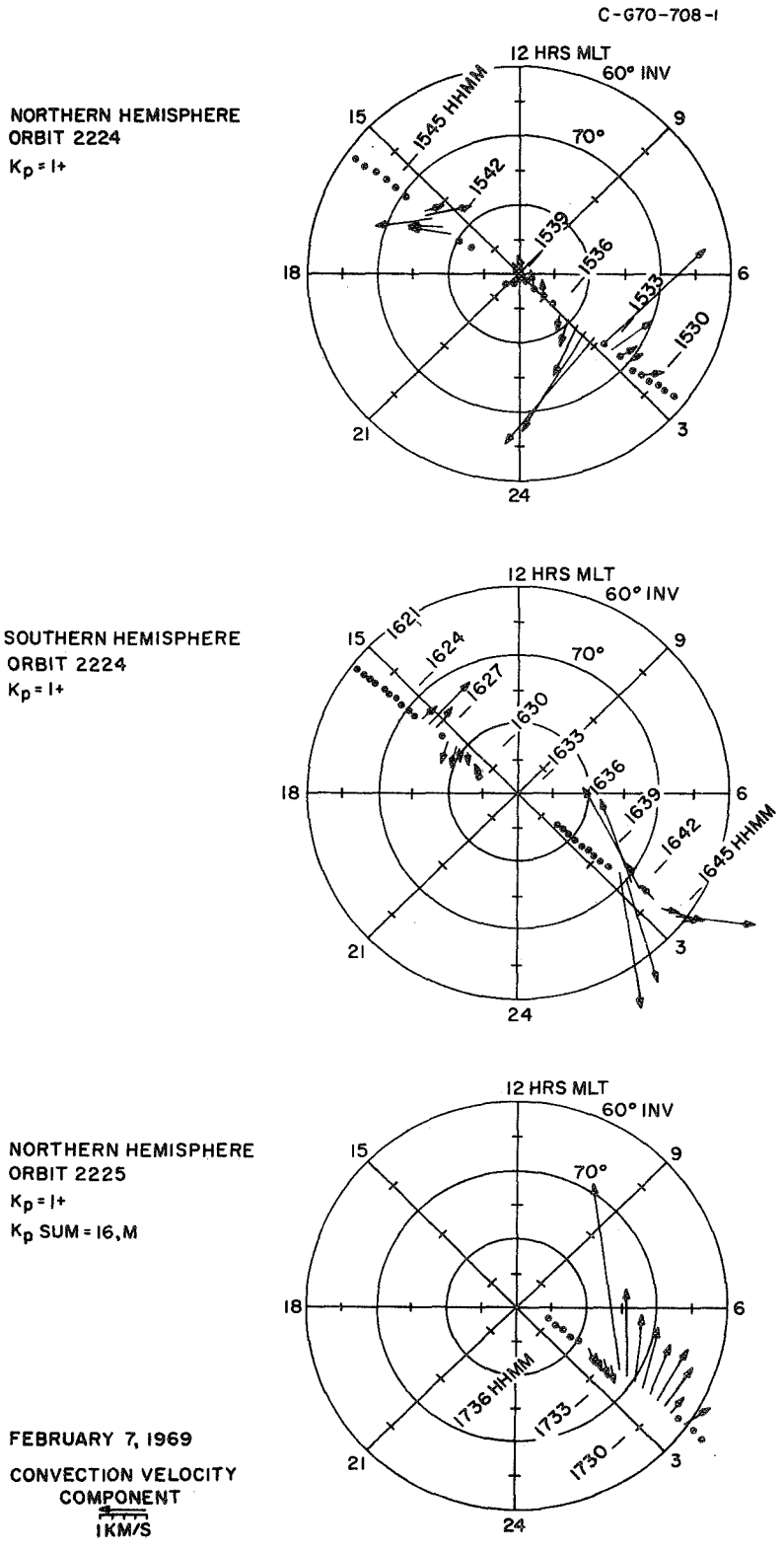
C-G70-708-1
NORTHERN HEMISPHERE
ORBIT 2224
Kp = 1+
12 HRS MLT
60° INV
70°
15
9
18
6
21
3
24
1545 HHMM
1542
1539
1536
1533
1530
SOUTHERN HEMISPHERE
ORBIT 2224
Kp = 1+
12 HRS MLT
60° INV
70°
1621
1624
1627
1630
1633
1636
1639
1642
1645 HHMM
NORTHERN HEMISPHERE
ORBIT 2225
Kp = 1+
Kp SUM = 16,M
12 HRS MLT
60° INV
70°
1736 HHMM
1733
1730
FEBRUARY 7, 1969
CONVECTION VELOCITY
COMPONENT
1KM/S

Figure 8

D-G70-665-I

ORBIT 6909
K_p = 3

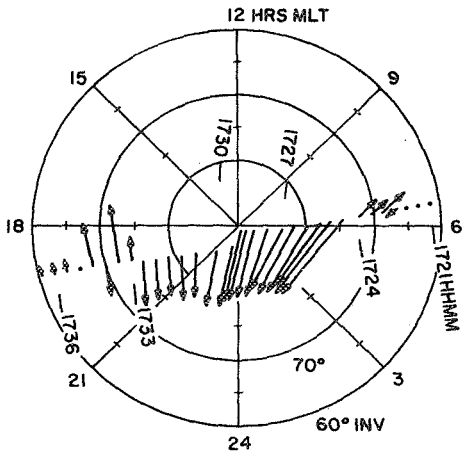

ORBIT 6910
K_p = 3

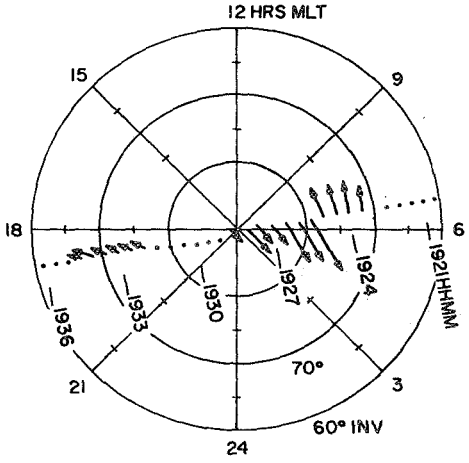

ORBIT 6911
K_p = 3+
K_p SUM = 14-

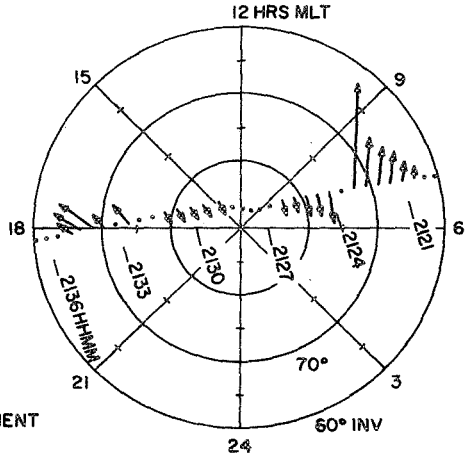

NORTHERN HEMISPHERE
FEBRUARY 27, 1970
ALTITUDE ~ 700KM

CONVECTION VELOCITY COMPONENT

1 KM/S

Figure 9

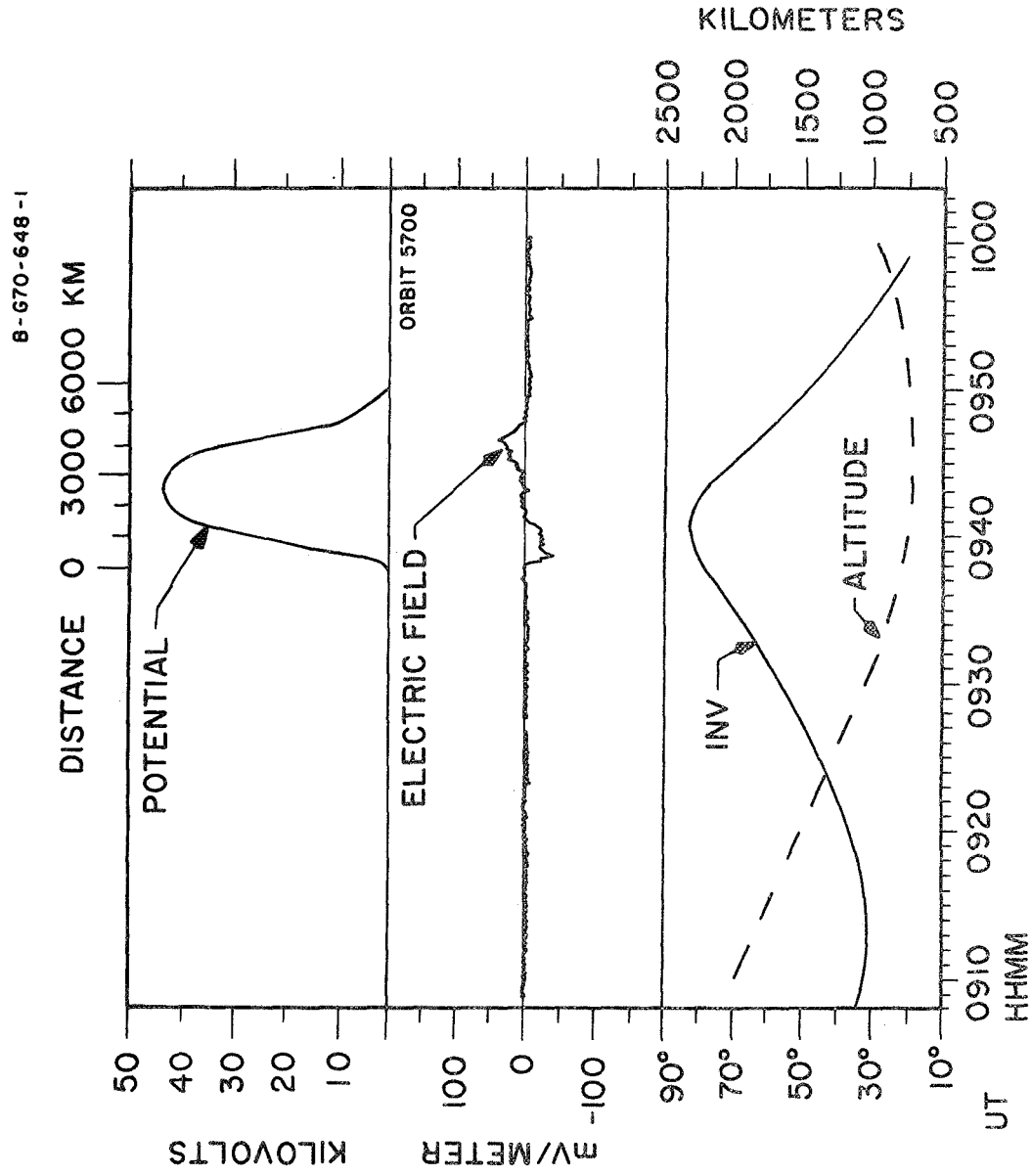
B-670-648-1
DISTANCE 0 3000 6000 KM
POTENTIAL
ELECTRIC FIELD
ORBIT 5700
INV
ALTITUDE
KILOVOLTS
mV/METER
KILOMETERS
UT
HHMM
MLT ~ 6.6 HRS
MLT ~ 18.6 HRS
K_p = 1-; K_p SUM = 8
SOUTHERN HEMISPHERE NOV. 20, 1969

Figure 10

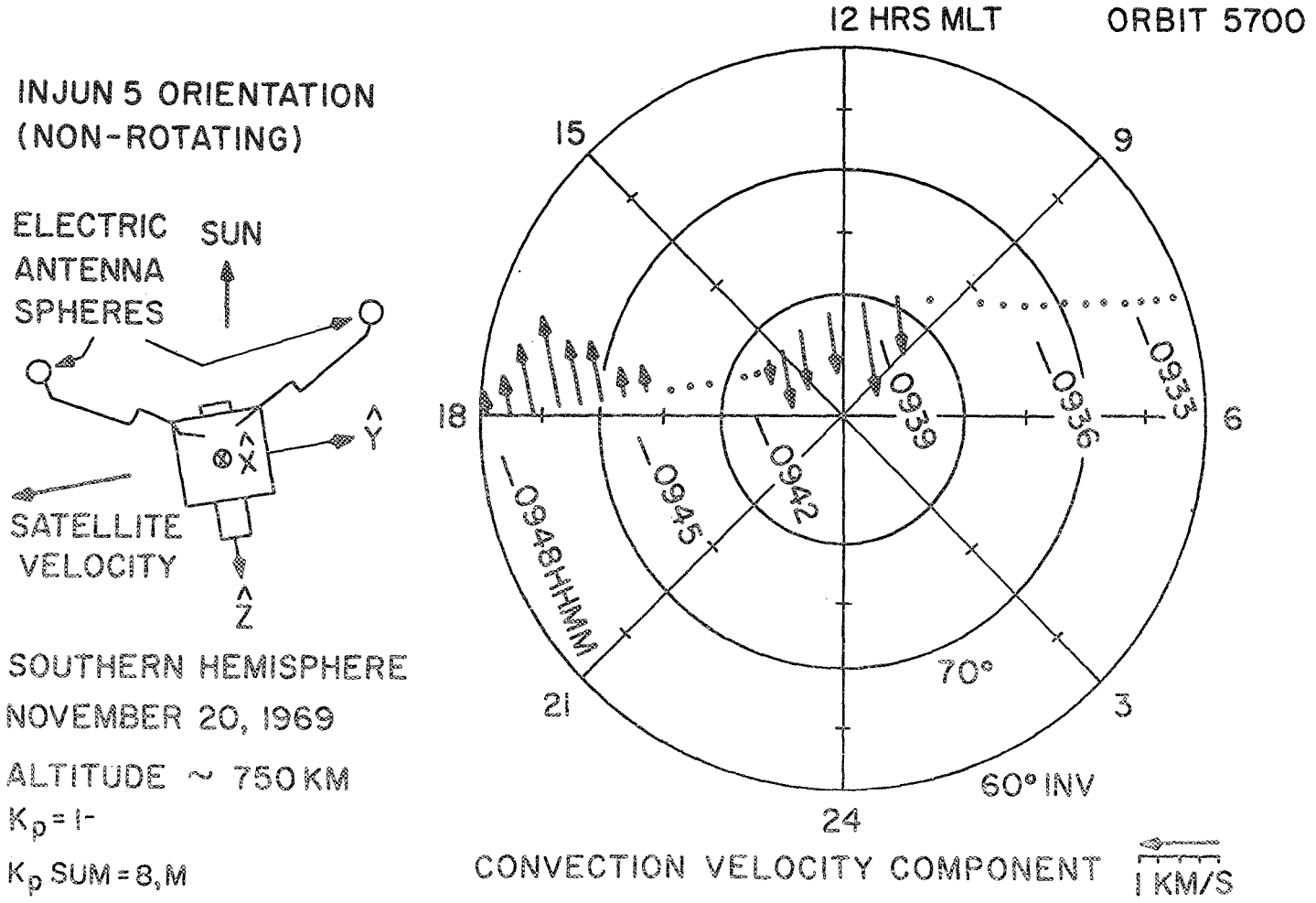
INJUN 5 ORIENTATION
(NON-ROTATING)
ELECTRIC
ANTENNA
SPHERES
SUN
Ŷ
X̂
SATELLITE
VELOCITY
Ẑ
SOUTHERN HEMISPHERE
NOVEMBER 20, 1969
ALTITUDE ~ 750 KM
K_p = 1-
K_p SUM = 8,M
12 HRS MLT
ORBIT 5700
15
9
18
6
21
3
24
0933
0936
0939
0942
0945
0948HHMM
70°
60° INV
CONVECTION VELOCITY COMPONENT
1 KM/S

Figure 11

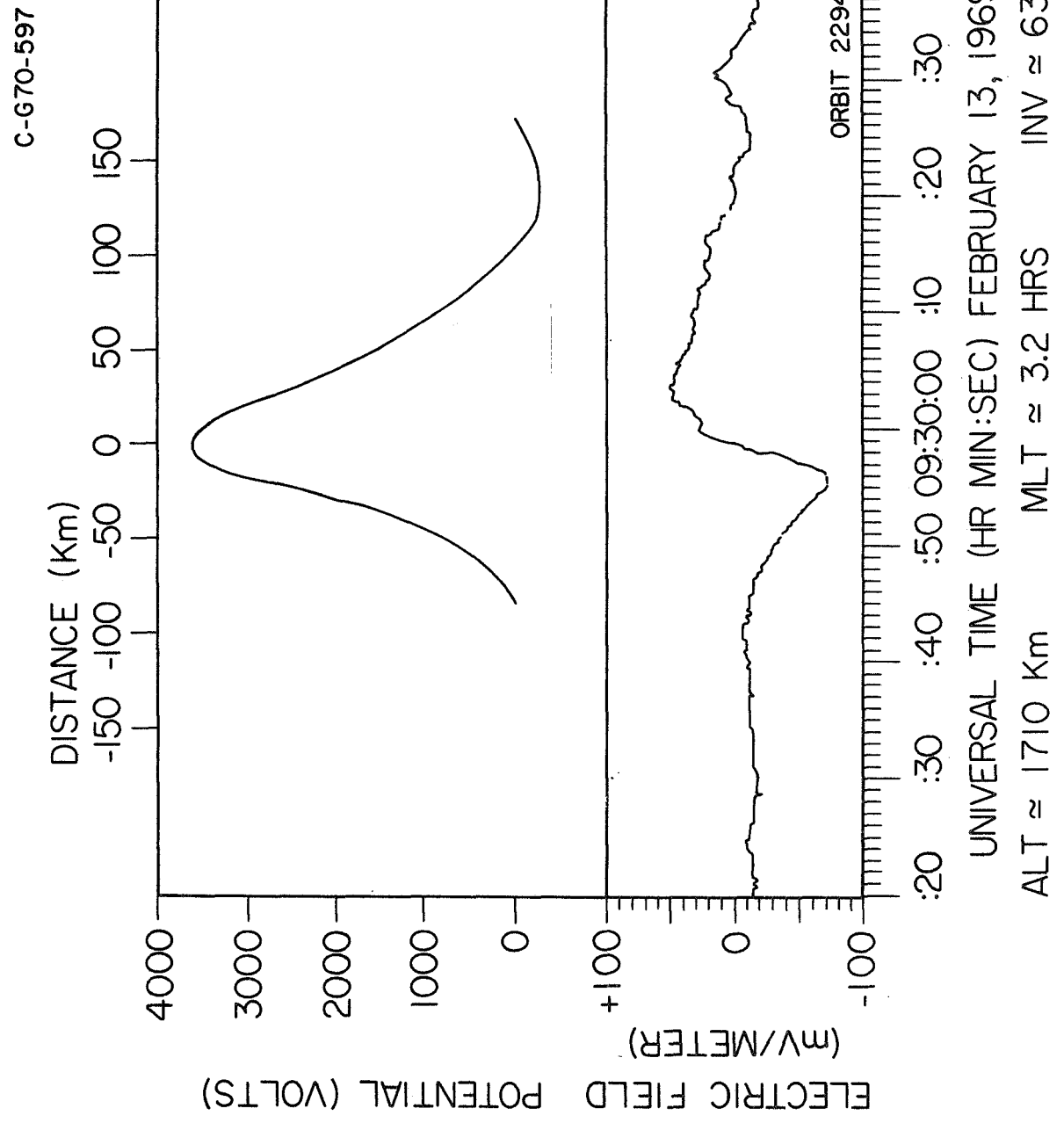
C-G70-597
DISTANCE (Km)
-150 -100 -50 0 50 100 150
4000
3000
2000
1000
0
ELECTRIC FIELD POTENTIAL (VOLTS)
+100
0
-100
(mV/METER)
ORBIT 2294
:20 :30 :40 :50 09:30:00 :10 :20 :30 :40
UNIVERSAL TIME (HR MIN:SEC) FEBRUARY 13, 1969
ALT ≈ 1710 Km MLT ≈ 3.2 HRS INV ≈ 63.3°

Figure 12

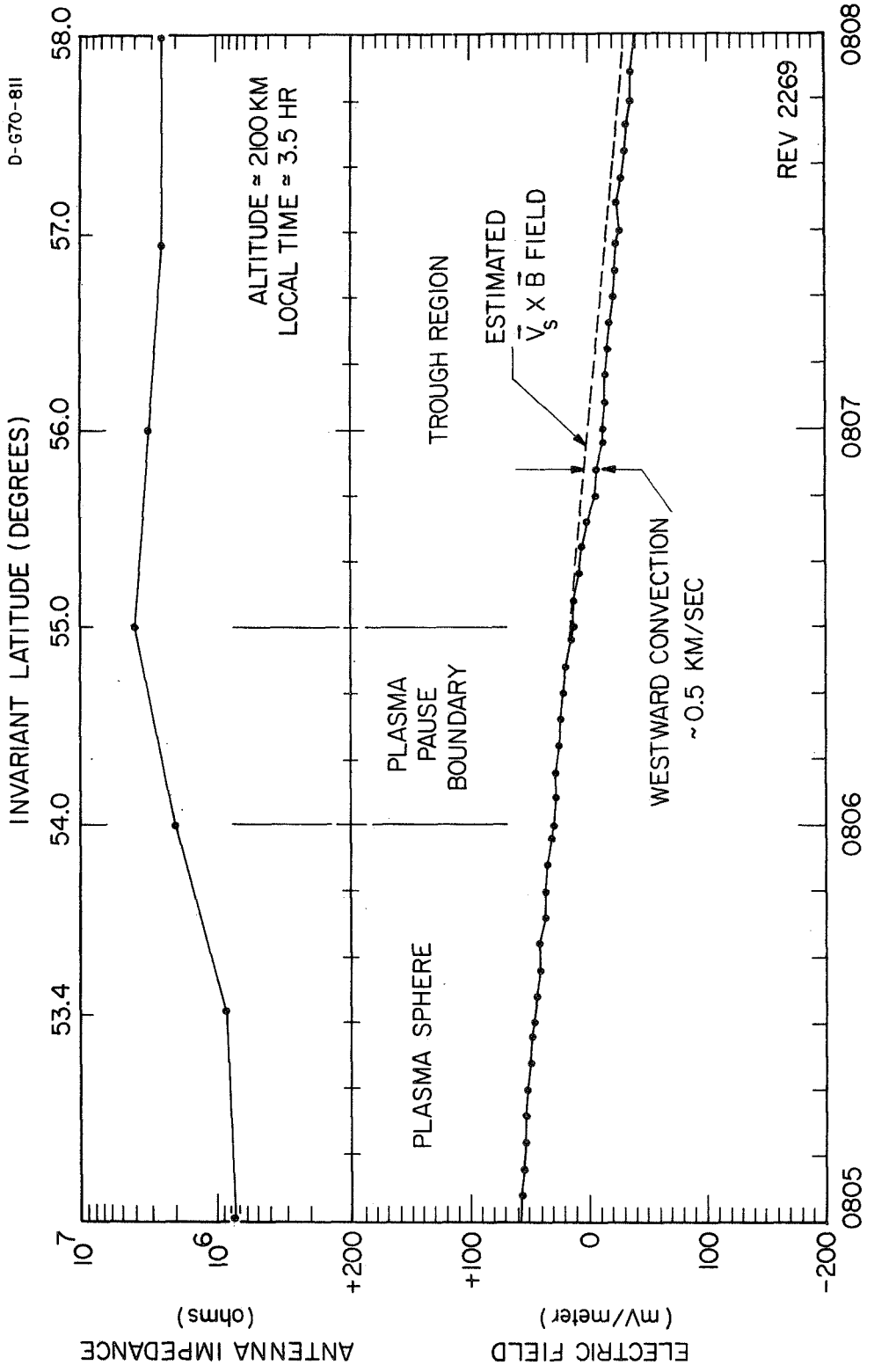
D-G70-811
INVARIANT LATITUDE (DEGREES)
53.4
54.0
55.0
56.0
57.0
58.0
ALTITUDE ≈ 2100 KM
LOCAL TIME ≈ 3.5 HR
PLASMA SPHERE
PLASMA PAUSE BOUNDARY
TROUGH REGION
ESTIMATED $\vec{V}_s \times \vec{B}$ FIELD
WESTWARD CONVECTION ~0.5 KM/SEC
REV 2269
ANTENNA IMPEDANCE (ohms)
10^7
10^6
ELECTRIC FIELD (mV/meter)
+200
+100
0
100
-200
0805
0806
0807
0808
UNIVERSAL TIME FEB. 11, 1969

Figure 13

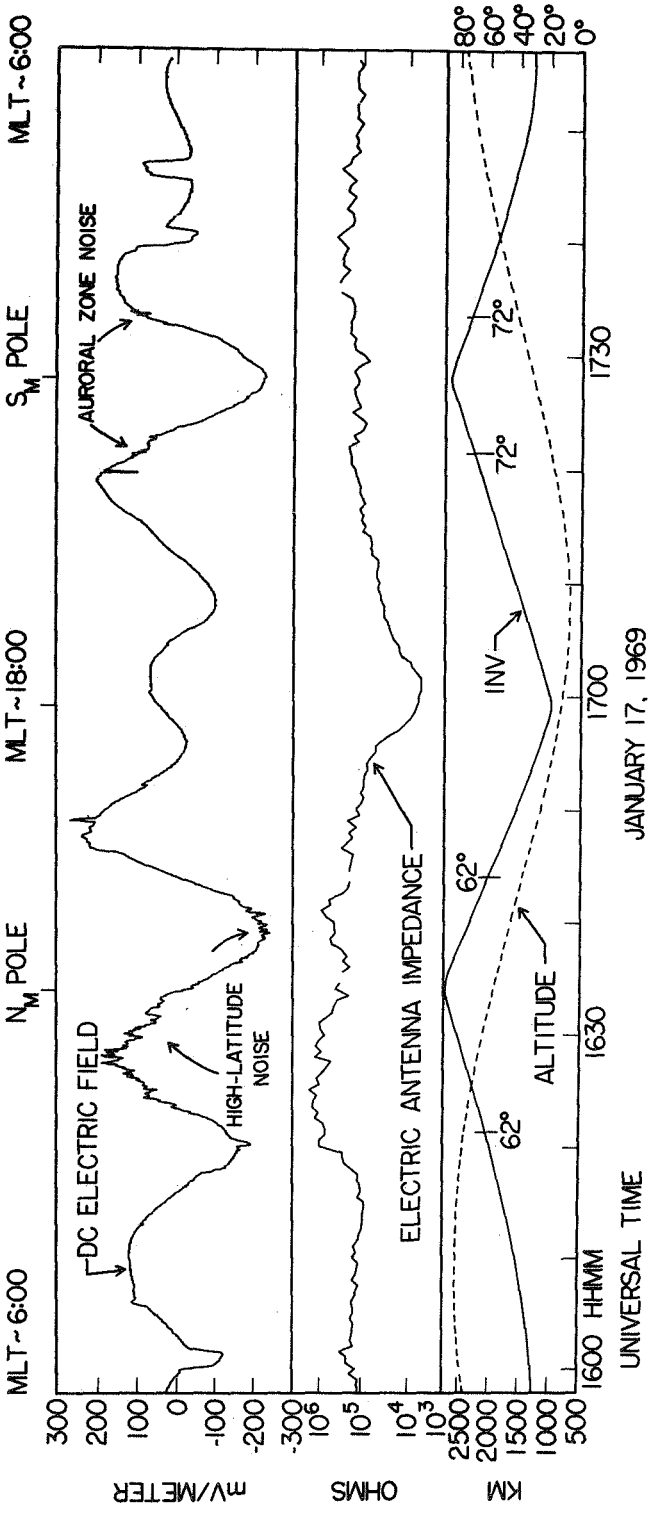
J-671-2
MLT~6:00
N_M POLE
MLT~18:00
S_M POLE
MLT~6:00
DC ELECTRIC FIELD
HIGH-LATITUDE NOISE
AURORAL ZONE NOISE
ELECTRIC ANTENNA IMPEDANCE
INV
ALTITUDE
62°
72°
80°
60°
40°
20°
0°
mV/METER
OHMS
KM
1600 HHMM
1630
1700
1730
UNIVERSAL TIME
JANUARY 17, 1969

Figure 14